CHANDRA
X-ray Center 60 Garden St., Cambridge Massachusetts 02138 USA

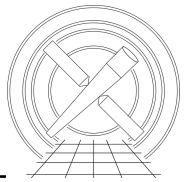

MEMORANDUM

Date: December 13, 2019
From: **Ping Zhao**
To: **CXC**
Subject: **Chandra Optical Axis and Aimpoint**
File: oxap_memo_2019.tex
Version: 22.0

Chandra X-ray Observatory revolutionized the X-ray astronomy as being the first, and so far the only, X-ray telescope achieving sub-arcsecond resolution. Chandra comprises of three principal elements: the High Resolution Mirror Assembly (HRMA), Pointing Control and Aspect Determination (PCAD) system, and the Science Instrument Module (SIM). To achieve and retain the unprecedented imaging quality, it is critical that these three principal elements stay rigid and stable for the entire life time of the Chandra operation. Measuring and tracking the telescope optical axis and aimpoint with respect to detector positions are the key to understand the stability of the telescope and to maintain the optimal Chandra operation.

This memorandum discuss the telescope focal-point, optical axis, aimpoint, their position drifts during the mission, the impact to Chandra operations, and mitigations.

1 Definitions

- **HRMA Optical Axis**: For ideal Wolter-I optics, the optical axis is defined by the axis of symmetry of the paraboloid and hyperboloid surfaces. For the actual HRMA, which is not made of perfect surfaces, the optical axis is a straight line passing through the geometric center of the four nested HRMA parabolic and hyperbolic surface mirror pairs and the HRMA focal point.
  - **HRMA Focal Point** (AKA HRMA Focus): Point on the focal plane where the sharpest PSF is located.
  - **HRMA Focal Plane**: An imaginary plane perpendicular to the HRMA optical axis and intersecting it at the focal point. (Note that the focal plane is not defined by the detector surface. Although placing the detector surface on or near the focal plane obtains the optimal on-axis imaging spatial resolution.)
- **ACA Reference Frame**: Frame based on the optical telescope Aspect Camera Assembly (ACA) pointing. The ACA reference frame is used to point the spacecraft. Any drift in the ACA to HRMA alignment will directly affect the actual location on the detector where an on-axis source lands.
- **HRMA Aimpoint**: Point on the focal plane where the image of an on-axis target is located (without detector offset).
  - **Effective Aimpoint**: Location on each detector where the image of an on-axis target actually landed. Effective aimpoint is not fixed and it actually drifts during the mission.

– **Default Aimpoint**: Fixed chosen locations on detectors to avoid the chip gaps and node boundaries while still maintaining the optimal PSF. Before cycle 18, default aimpoints on ACIS-I and ACIS-S were managed by setting certain pointing offset annually to compensate the slow drift of the effective aimpoint. Starting with Cycle 18 observations, a permanent default aimpoint (PDA) is chosen for each detector without using the offset (see Section 8).

For ideal mirrors, the optical axis intersects the focal plane at the best focus which is both the focal point and the aimpoint. For the actual HRMA, the focal point and the aimpoint are not the same, although they differ only slightly. With respect to a preset coordinate system associated with each detector, the positions of both points have been drifting slowly since launch. The focal point (i.e. optical axis) drift is due to the alignment between the HRMA and the focal plane instruments. The aimpoint drift is due to the alignment between the HRMA and ACA.

2 Telescope Pointing

The telescope pointing, i.e. the target acquisition, is accomplished through the following steps, as illustrated by Figure 1 (refer POG Figure 5.3):

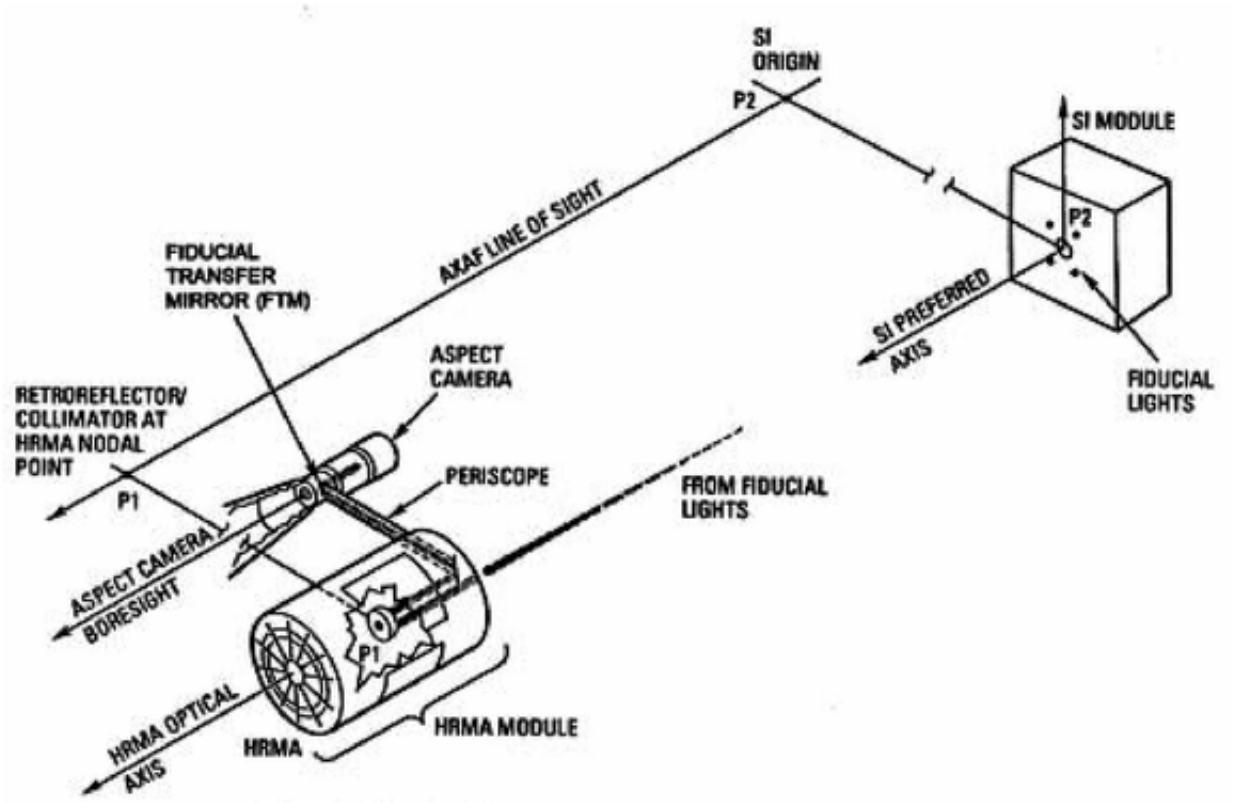

Figure 1: Chandra Pointing and Fiducial Transfer System. (POG: Figure 5.3.)

1. Target coordinate: the target coordinate is requested by the observer, which is registered as (RA_targ, Dec_targ) in the data header.

2. ACA attitude (Aspect Camera Assembly pointing): based on the target coordinate (RA_targ, Dec_targ), the ACA pointing (command position) is computed in terms of quaternions, which are registered in the ACA database. There is an 89.6″ offset between the target position and ACA pointing, due to the pre-launch ACA alignment.

3. Telescope attitude (HRMA pointing): once the ACA is pointed to its command position, the HRMA is automatically pointed to (RA_pnt, Dec_pnt), which is the computed mean pointing of the (dithered) observation. This information is registered in the data header. There is a ∼97″ offset between the HRMA pointing and the ACA pointing.

4. Target position: once the HRMA is pointed to (RA_pnt, Dec_pnt), the image of an on-axis target will be at the aimpoint[1], which has the observer requested coordinates (RA_targ, Dec_targ). There is a ∼17″ offset between (RA_pnt, Dec_pnt) and (RA_targ, Dec_targ).

3 Aimpoint on Chandra Detectors

For each Chandra observation, one of four Chandra detectors is aligned with the HRMA optical axis by moving the entire Science Instrument Module (SIM) to that detector's nominal SIM-Z position. Figure 2 shows the layout of Chandra detectors in the SIM plane with the aimpoints indicated at their nominal positions.

[1]Since the Chandra spacecraft has a built-in dither (of Lissajous figure with peak-to-peak amplitude of 16″ for ACIS and 40″ for HRC) on its pointing position to average across calibration uncertainties, the aimpoint is actually the center of the dither pattern.

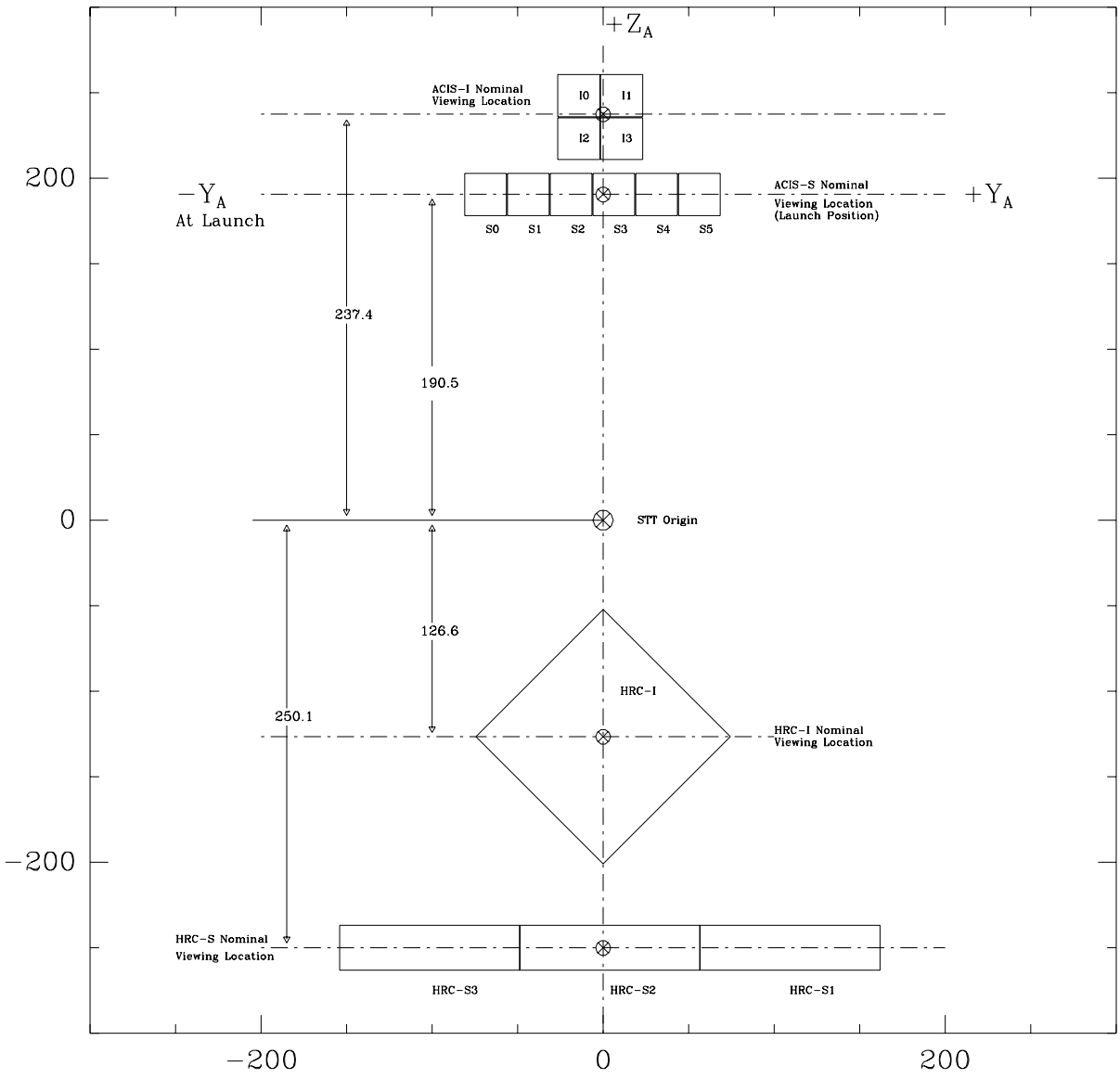

Figure 2: Chandra Detectors Layout: The schematic of the SIM plane shows the Chandra focal plane instrument to scale (in mm, coordinate system is AXAF-STT-1.0). SIM +Y is along the x-axis; SIM +Z is along the y-axis. ⊗ on each detector marks the aimpoint position with nominal SIM-Z position and zero pointing offset.

4 Optical Axis and Aimpoint Drifts

Both the optical axis and the aimpoint have been drifting in the SIM plane since the Chandra launch. Their relative positions change continuously. Their positions on each detector are critical for the optimal operation of the Chandra X-ray Observatory. Therefore the positions of both points are continuously monitored.

4.1 Optical Axis Drift

The optical axis position is derived from semi-annual annular scan observations of Ar Lac, an eclipsing RS CVn binary star, using the HRC-I detector. The annular scan is a set of observations with one exposure at the aimpoint and a set of exposures on rings centered at the aimpoint and with $1', 2', 3', 4', 6'$ radii and 45° azimuthal increments for a total of 42 observations each year, 21 of them were carried out every half year and with 45° azimuthal offset from each other. Figure 3 shows the annular scan pattern.

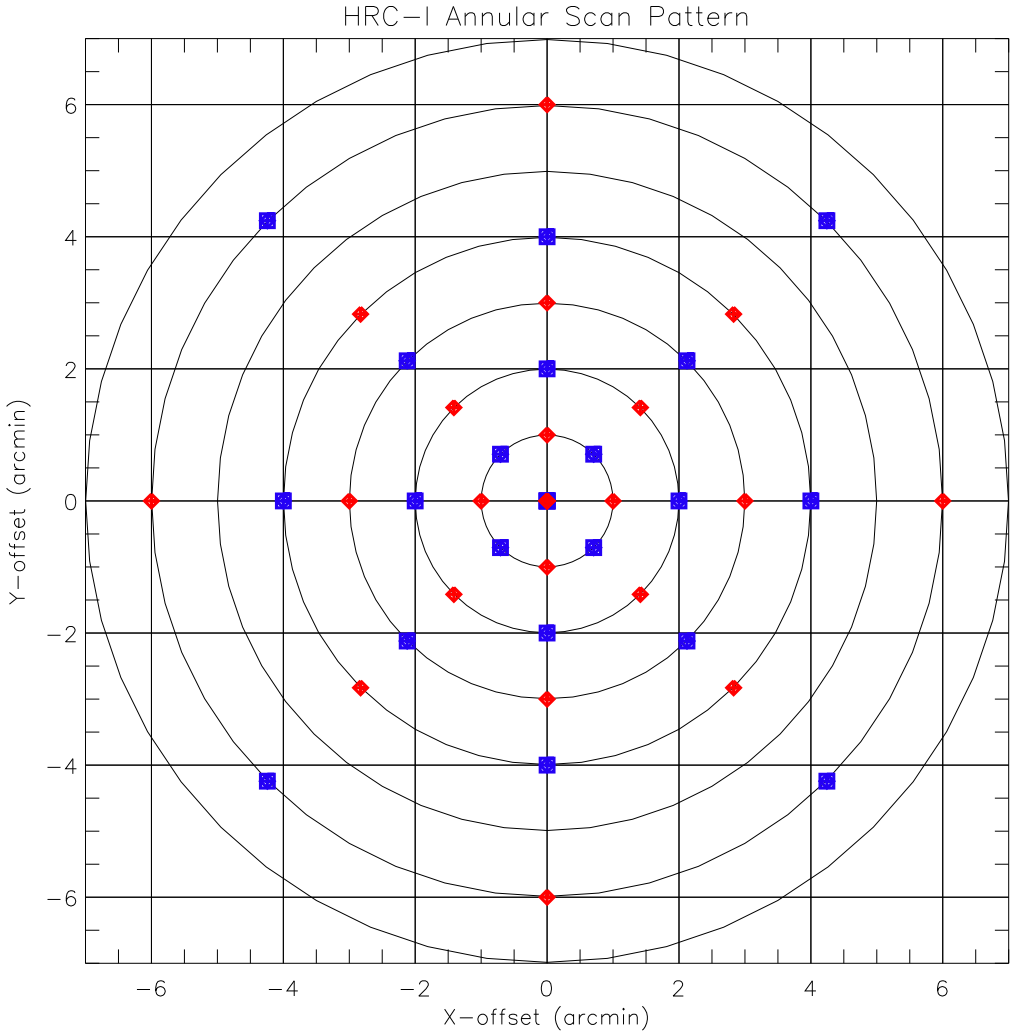

Figure 3: The annular scan pattern of Ar Lac using the HRC-I detector: The red diamond positions were scanned in April; the blue square positions were scanned in September, with 21 observations in each scan. The center (aimpoint) position has 5 ks exposure time; other positions have 1 ks exposure time.

As the observations go off-axis, their image encircled energy radii become larger and larger. The optical axis is determined by fitting the encircled energy radii (r) from each annular scan observation to the following 2-dimensional quadratic function in detector coordinates. By definition, the focal point is where the quadratic function is at its minimum and the optical axis goes through this point.

$$r = ax^2 + bxy + cx^2 + dx + ey + f \tag{1}$$

where x and y are the chip coordinates [X, Y]; r is the encircled energy radius; a, b, c, d, e, f are the fitting constants.

Figure 4 and 5 show the annular scan data taken in April and September 2019, respectively. The five circles around each data point indicate the 50%, 60%, 70%, 80% and 90% encircled energies. For clarity, the circle radii are 5 times the actual encircled energy radii. By definition, the optical axis is at the position (x_0, y_0) where the quadratic function is at its minimum ($r_{min} = r_0(x_0, y_0)$).

Figure 6 and 7 shows the optical axis derived from equation (1) using the April and September 2019 data.

Figure 8 shows all the optical axis positions so determined since the *Chandra* launch. They are quite stable, staying well within a $10''$ region and consistent with the measurement errors. This indicates that the optical bench connecting the HRMA and the SIM is rigid and the alignment between the two is very stable. The HRMA PSF and therefore the superb *Chandra* imaging resolution has been consistent since the *Chandra* launch.

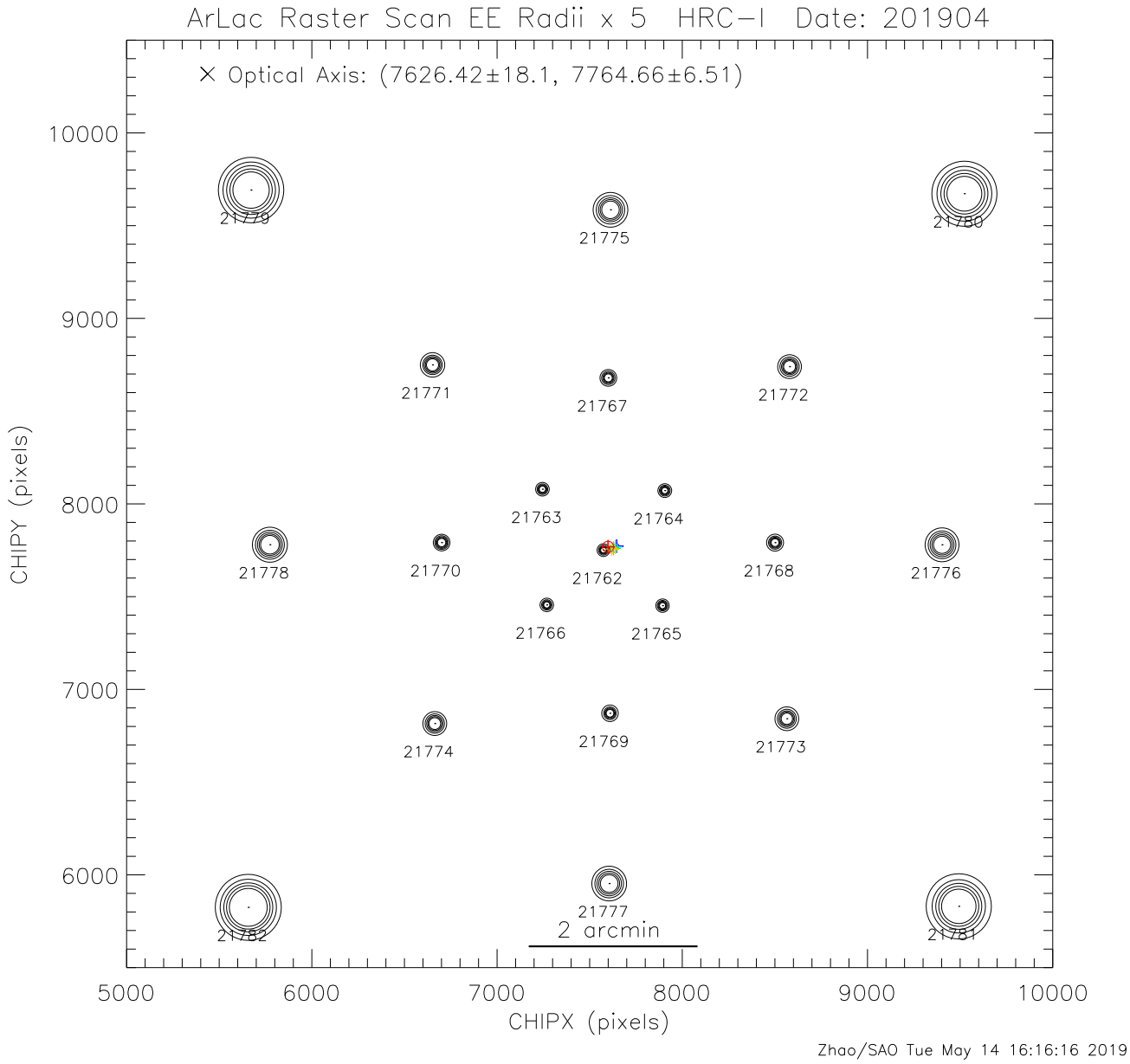

Figure 4: HRC-I annular scan observation of Ar Lac in chip coordinates. Circles around each observation point have the 50% – 90% encircled energy radii × 5. The data are fit to a 2-D quadratic function to find the optical axis. Data taken in April 2019. The numbers under the circles are the OBSIDs of the observations.

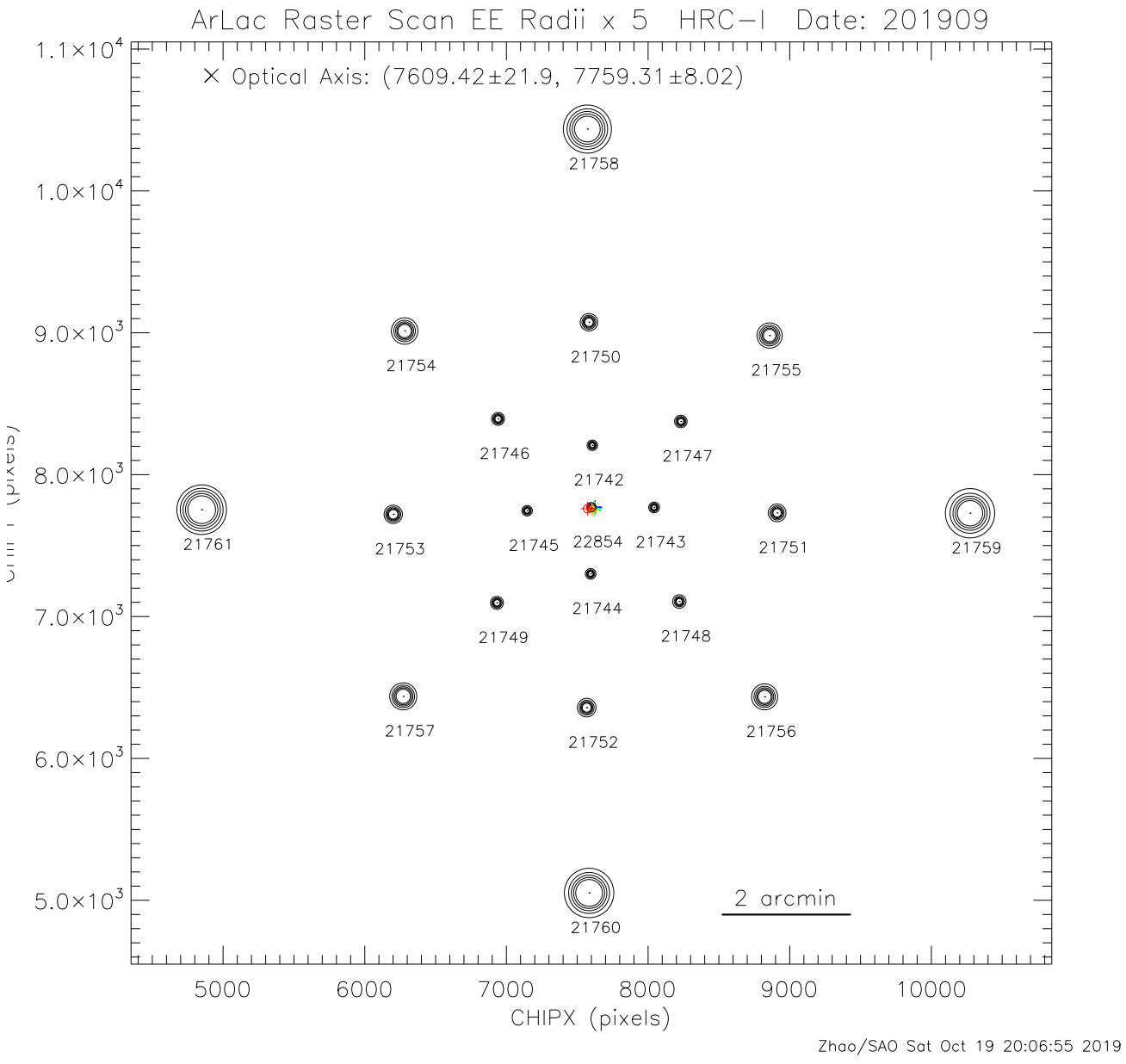

Figure 5: HRC-I annular scan observation of Ar Lac in chip coordinates. Circles around each observation point have the 50% – 90% encircled energy radii × 5. The data are fit to a 2-D quadratic function to find the optical axis. Data taken in September 2019. The numbers under the circles are the OBSIDs of the observations.

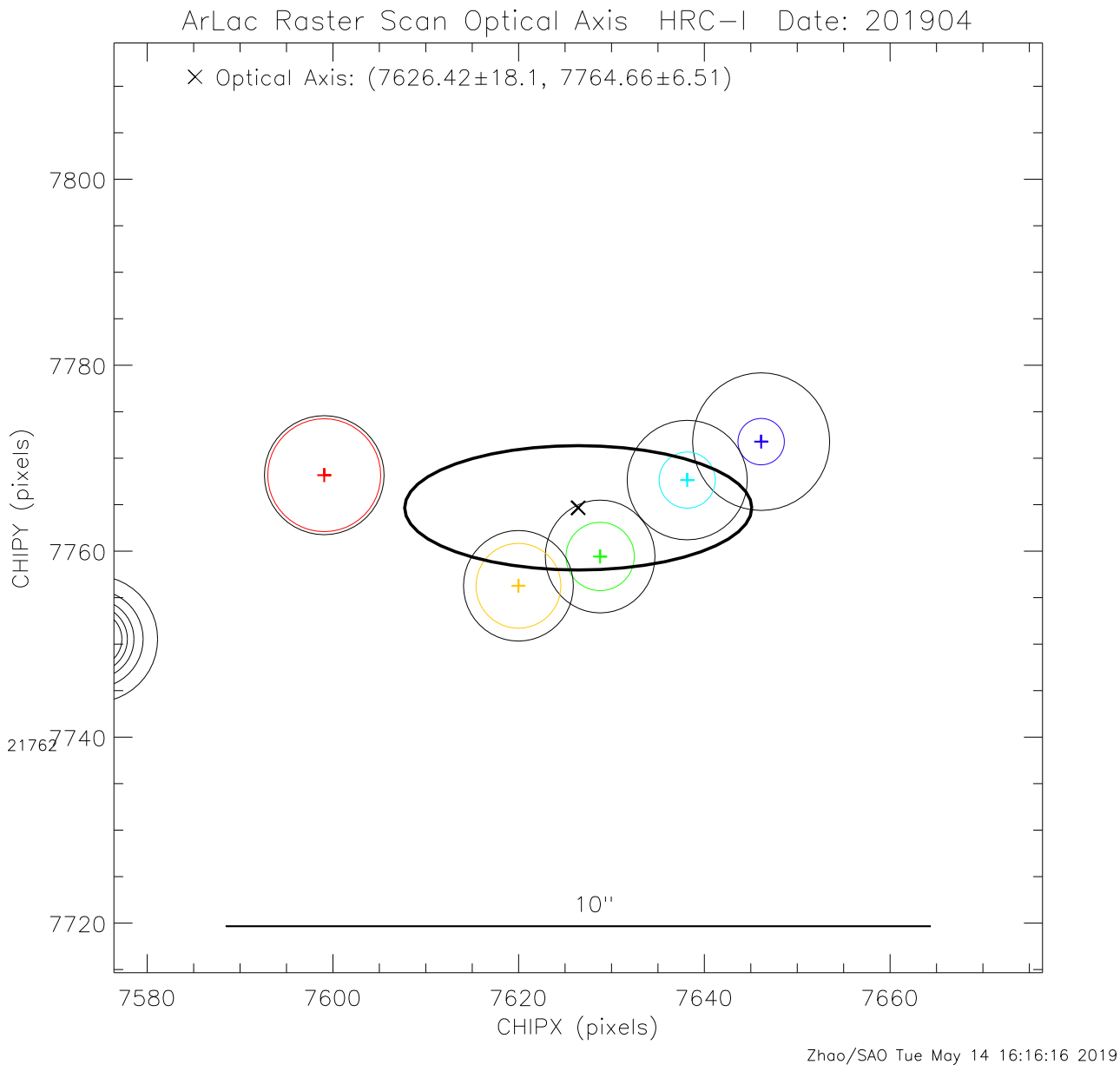

Figure 6: Same as Fig. 4 but zoomed in to the optical axis region. The five colored ×'s are the positions of quadratic function minimum for 50% – 90% encircled energy fit. The colored circles indicate their encircled energy radii. The black circles are the 1-σ fit errors. The black × marks the optical axis position, taken as the mean of the above 5 minimums. The black oval is the 1-σ error ellipse.

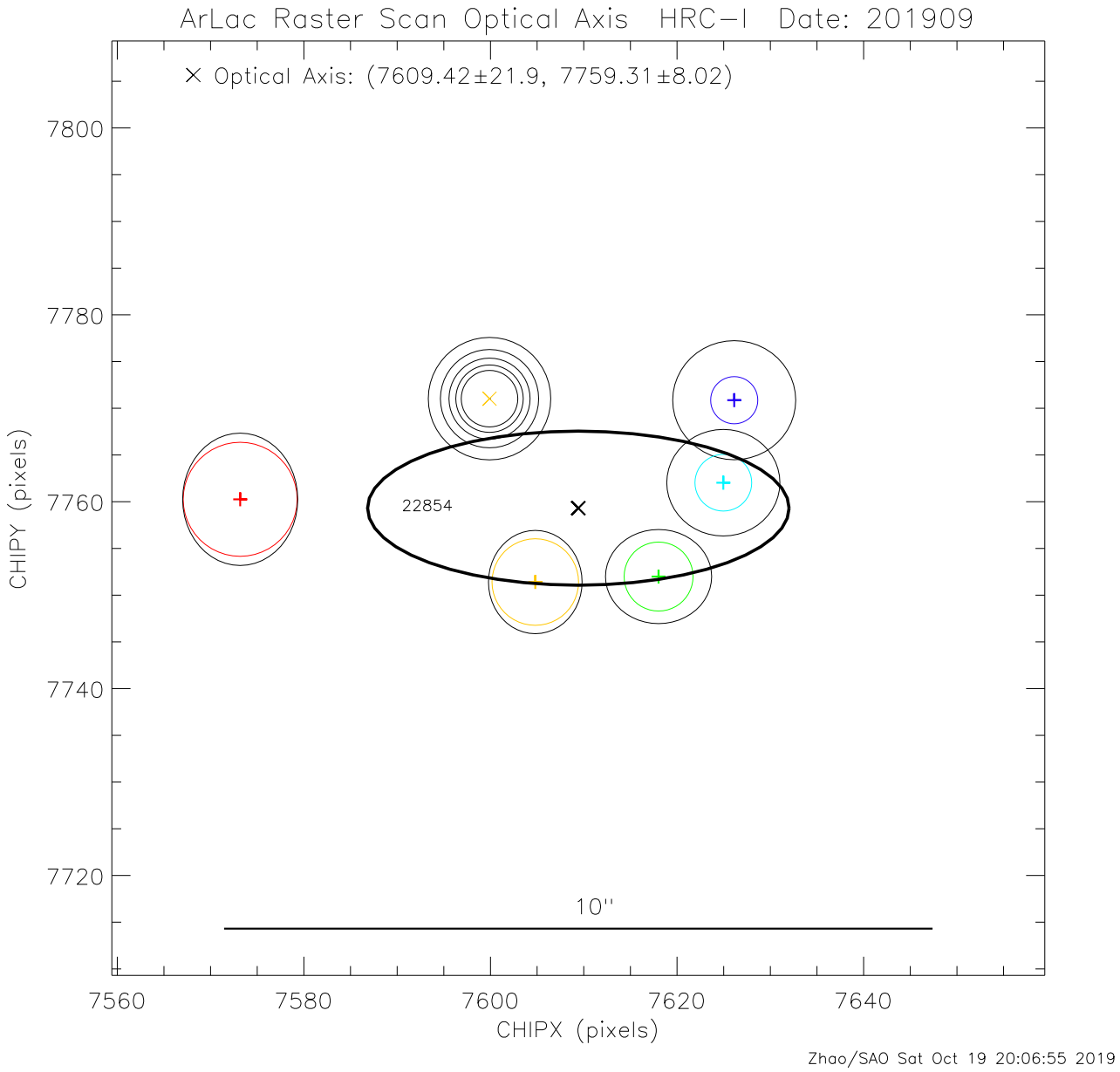

Figure 7: Same as Fig. 4 but zoomed in to the optical axis region. The five colored ×'s are the positions of quadratic function minimum for 50% – 90% encircled energy fit. The colored circles indicate their encircled energy radii. The black circles are the 1-σ fit errors. The black × marks the optical axis position, taken as the mean of the above 5 minimums. The black oval is the 1-σ error ellipse. The x above the black oval and the circles around it are the 5 ks on-axis observation (OBSID 22845) and its 50% – 90% encircled energy radii ×5.

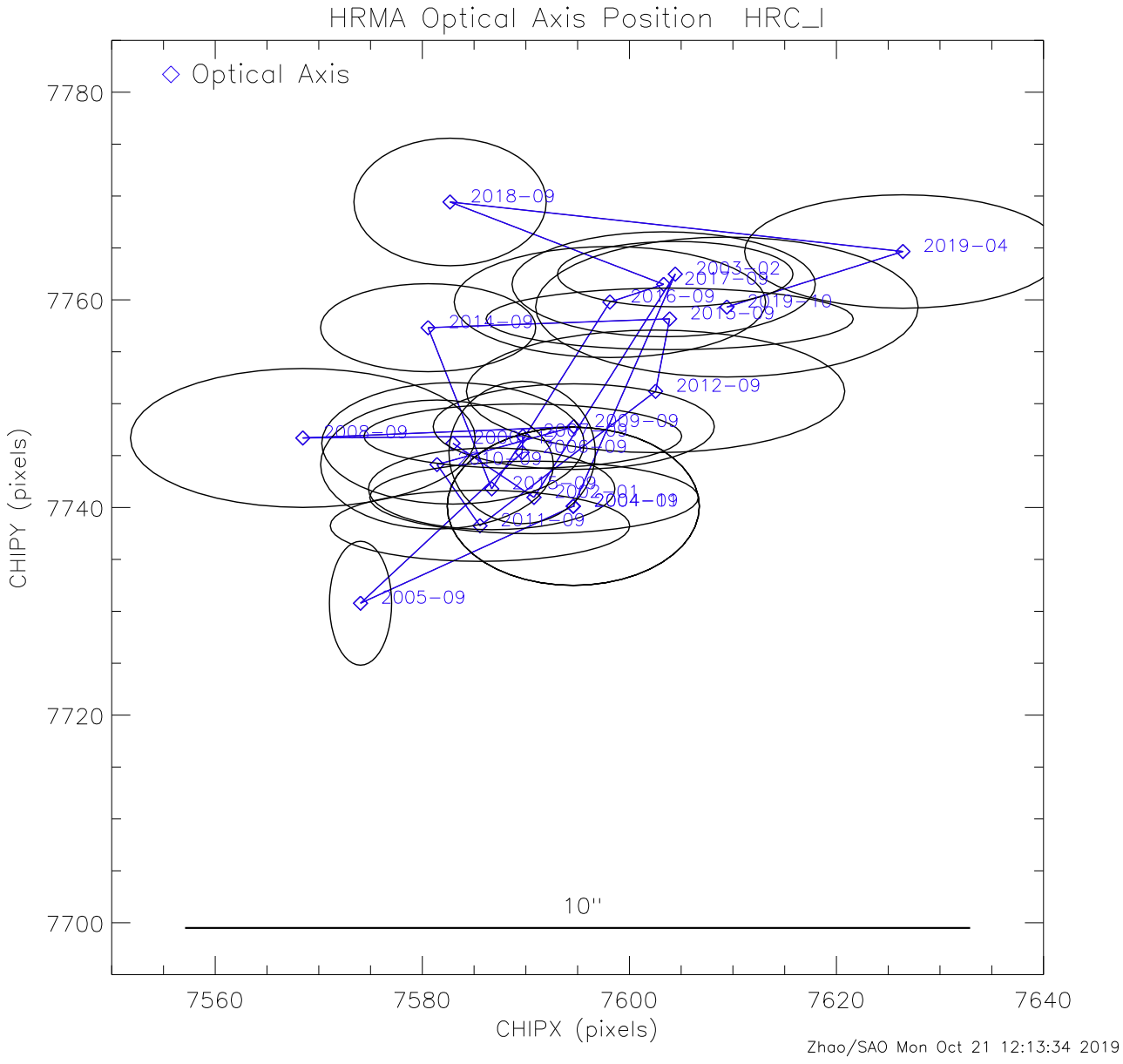

Figure 8: Chandra optical axis positions on HRC-I since launch. Each position is labeled by the year–month. The ellipse around each position is the $1-\sigma$ measurement error ellipse for that given year. The drift of optical axis position is consistent with the measurement errors. The optical axis position is very stable and well within a $10''$ region.

4.2 Aimpoint Drift

Aimpoint drift is largely due to changes in the alignment between the X-ray telescope (HRMA) and the optical telescope (Aspect Camera Assembly – ACA). As the spacecraft pointing and attitude determination is referenced to the ACA frame, when the alignment between that frame and the HRMA optical axis changes, the effective aimpoint drifts. Changes in that alignment have been seen over the long and short term, and in discrete jumps.

Since launch, the Chandra aimpoint has been drifting in the SIM [−Y,−Z] direction. Figures 9 – 16 show the aimpoint (with zero offset) positions of all the Chandra observations, on all four detectors in chip coordinates as a function of time since launch (and in the past three years). It is seen that the aimpoint has been drifting in the SIM [−Y,−Z] direction from 1999 until the beginning of year 2011. During that period, there are two relatively large shifts in June 2003 and November 2006, which are due to the ACA cool-down. Then in early 2011, the aimpoint drift reversed its direction, especially after the safemode in July 2011. In early 2012, the aimpoint drift is again back to its original trend in the SIM [−Y,−Z] direction. Since the late 2014, the drift is reversed again. At the same time, the drifting rate has accelerated and the short-term fluctuations has increased, due to the decreasing thermal stability in the ACA housing.

From launch to the the end of 2014, the aimpoint drifted about 30″. From January to November of 2015, the aimpoint drifted about 8″ in the reverse direction. There are two possible effects due to the aimpoint drift: 1) If the aimpoint drifted too far from the optical axis, the PSF may be degraded; 2) For the ACIS detectors, the drift may cause the on-axis target to fall off the chip edge (ACIS-I) or cross the node boundary (ACIS-S). So far the maximum drift was only 30″, and at no time the separation between the aimpoint and optical axis have been more than 27″. Since this is relatively small compared to the offaxis angle at which the PSF starts to degrade (See POG Figures 4.12 and 4.13), the PSF of near axis sources has stayed the same during the entire Chandra operation. So the first possible effect is not a concern.

To mitigate the second effect, during Cycles 1 through 17, the default target offsets were updated for each proposal cycle for ACIS observations by assigning a series default offsets based on their then zero offset aimpoint chip positions, effectively compensating for ACA/optical axis alignment drift and placing the default aimpoint away from chip edges or node boundaries and closer to the optical axis. Since 2014, however, the overall ACA temperature and its short term fluctuations have increased, and thus temperature-driven changes in alignment have become larger and changed more quickly. Thus using the default offsets set in a yearly basis is no longer adequate to ensure the proper aimpoint position.

To compensate for these more dynamic changes, starting with Cycle 18 observations, we used recent ACA/HRMA alignment data during the PCAD attitude planning process, altering the ACA/spacecraft pointing to adjust for new alignment drift, and thus fixing or pinning the placement of the effective aimpoint. Default offsets will no longer be needed to compensate for alignment changes, instead a permanent default aimpoint is chosen for each detector, which will be set dynamically (see Section 8).

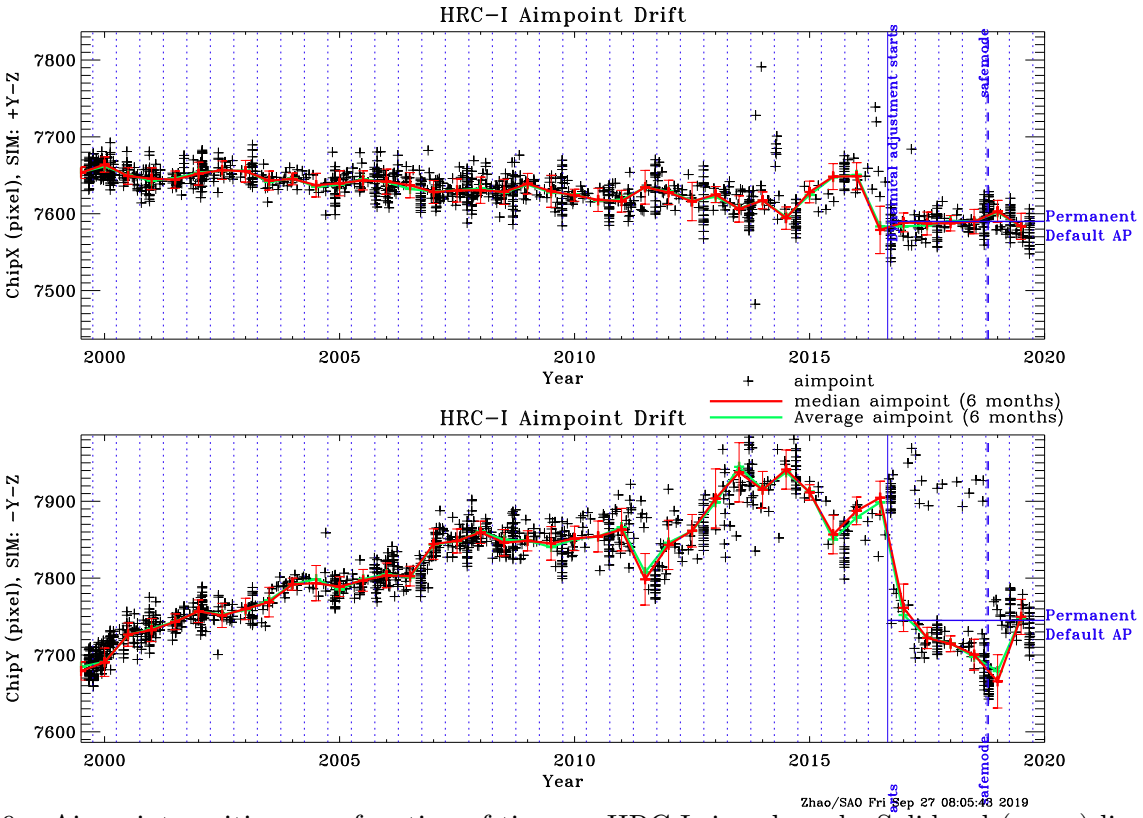

Figure 9: Aimpoint position as a function of time on HRC-I since launch. Solid red (green) lines show the median (average) aimpoint drift in 6 month bins, separated by vertical dotted blue lines. The vertical solid blue line indicates the start of the dynamical aimpoint adjustment.

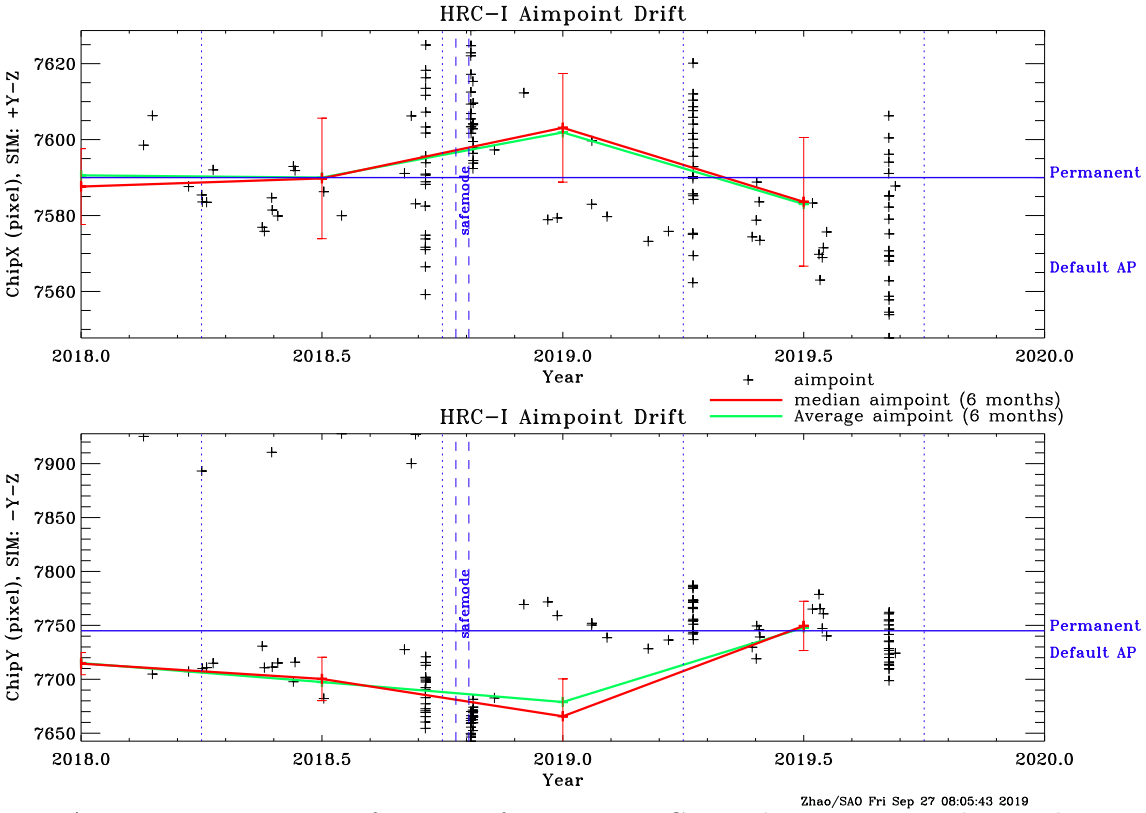

Figure 10: Aimpoint position as a function of time on HRC-I in the past year. The gap between the two vertical dashed lines indicate when Chandra was in safemode (Oct. 10–21, 2018).

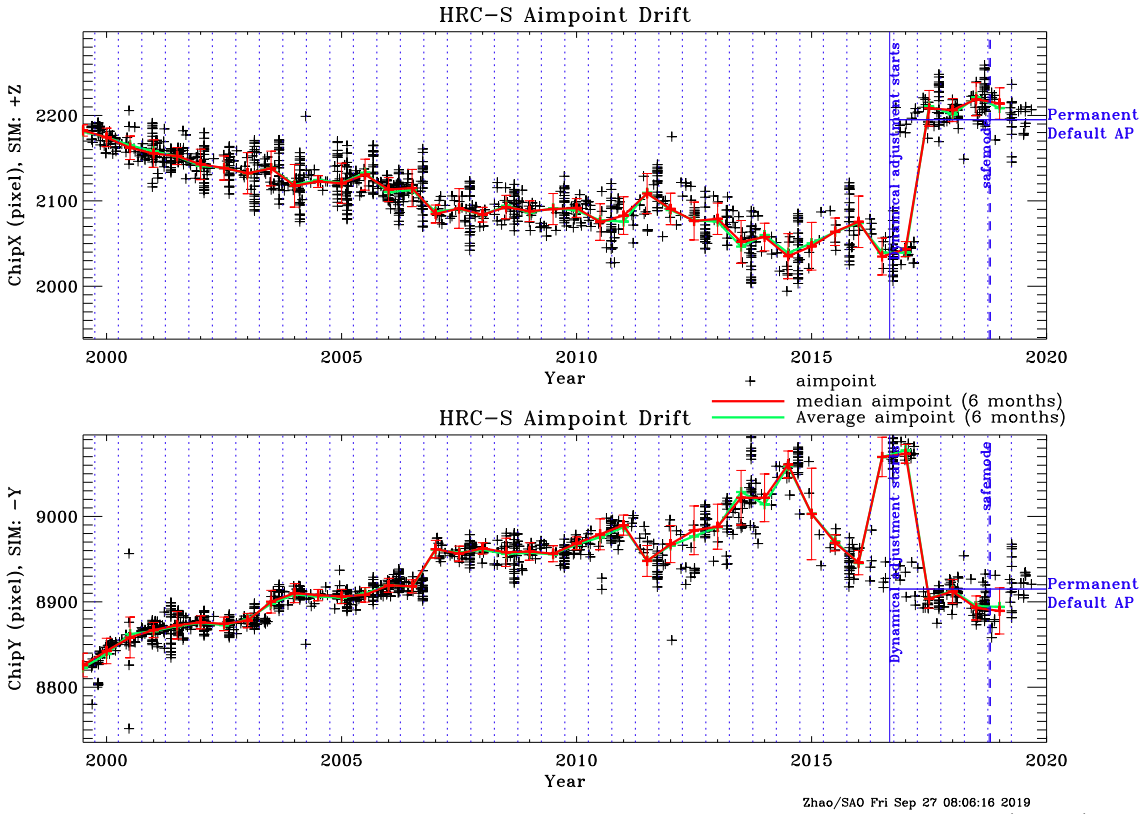

Figure 11: Aimpoint position as a function of time on HRC-S since launch. Solid red (green) lines show the median (average) aimpoint drift in 6 month bins, separated by vertical dotted blue lines. The vertical solid blue line indicates the start of the dynamical aimpoint adjustment.

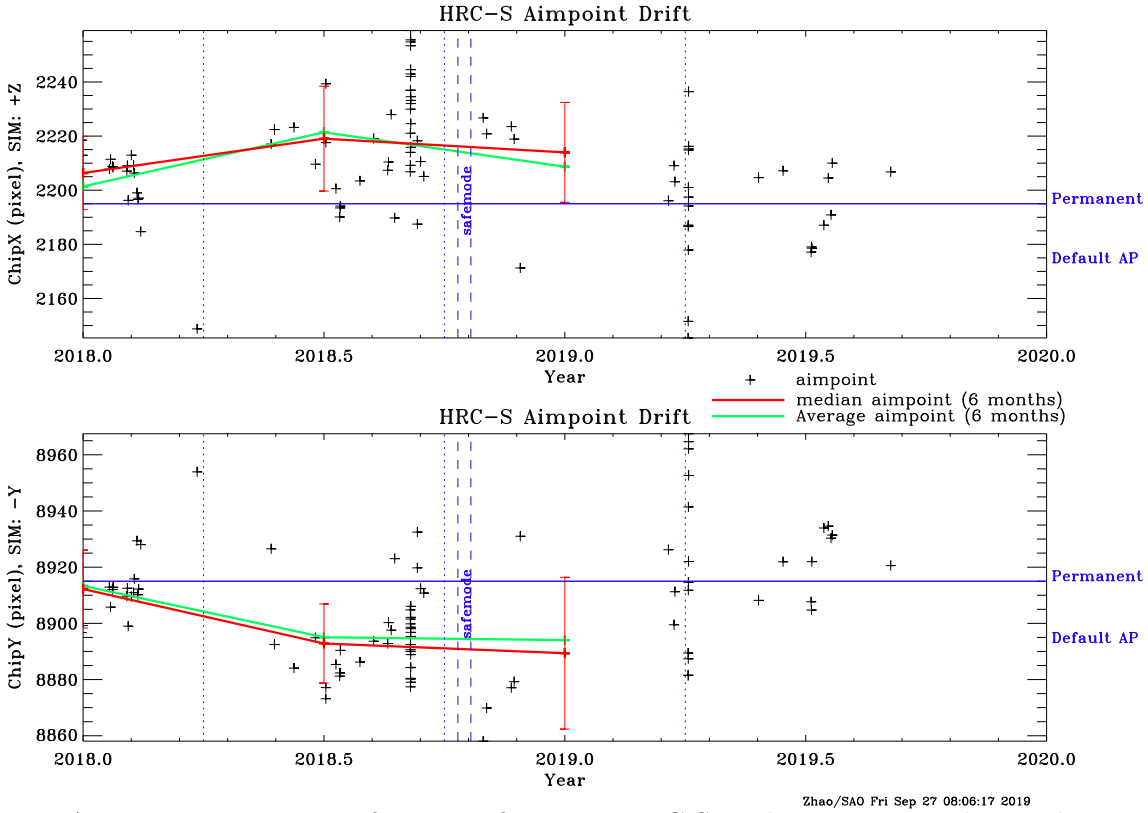

Figure 12: Aimpoint position as a function of time on HRC-S in the past year. The gap between the two vertical dashed lines indicate when Chandra was in safemode (Oct. 10–21, 2018).

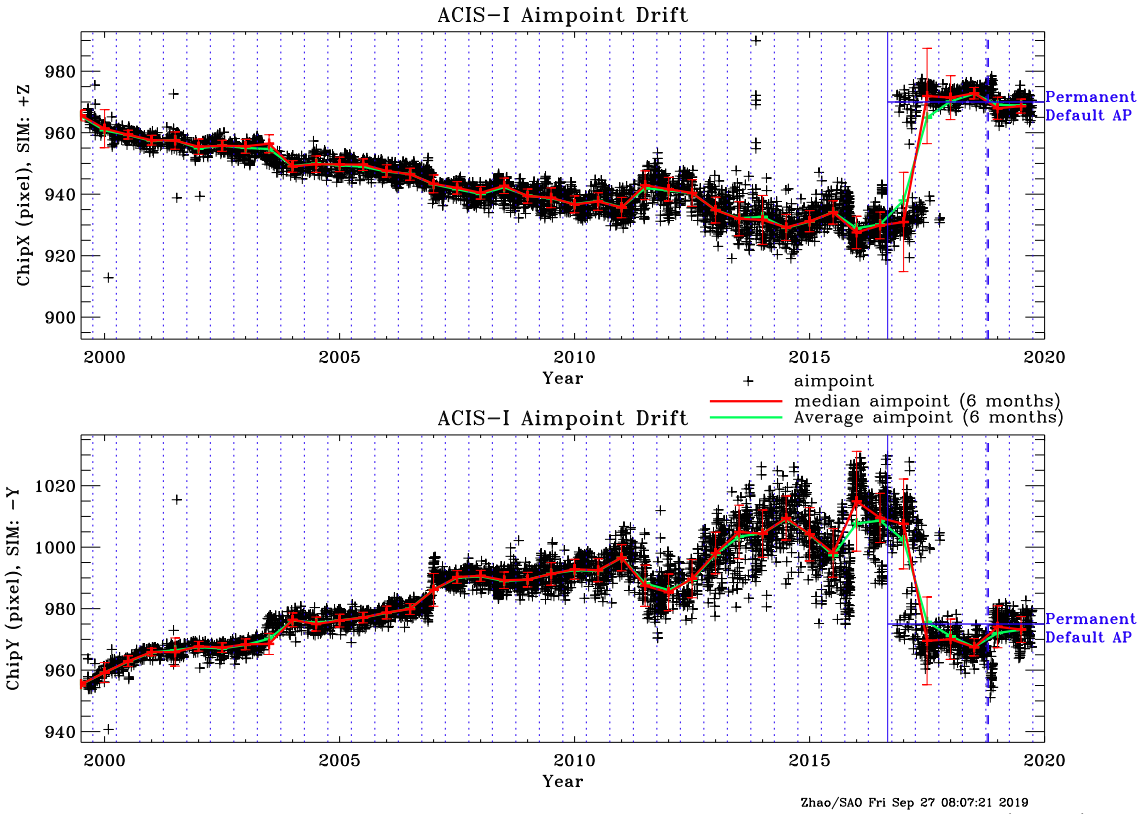

Figure 13: Aimpoint position as a function of time on ACIS-I since launch. Solid red (green) lines show the median (average) aimpoint drift in 6 month bins, separated by vertical dotted blue lines. The vertical solid blue line indicates the start of the dynamical aimpoint adjustment.

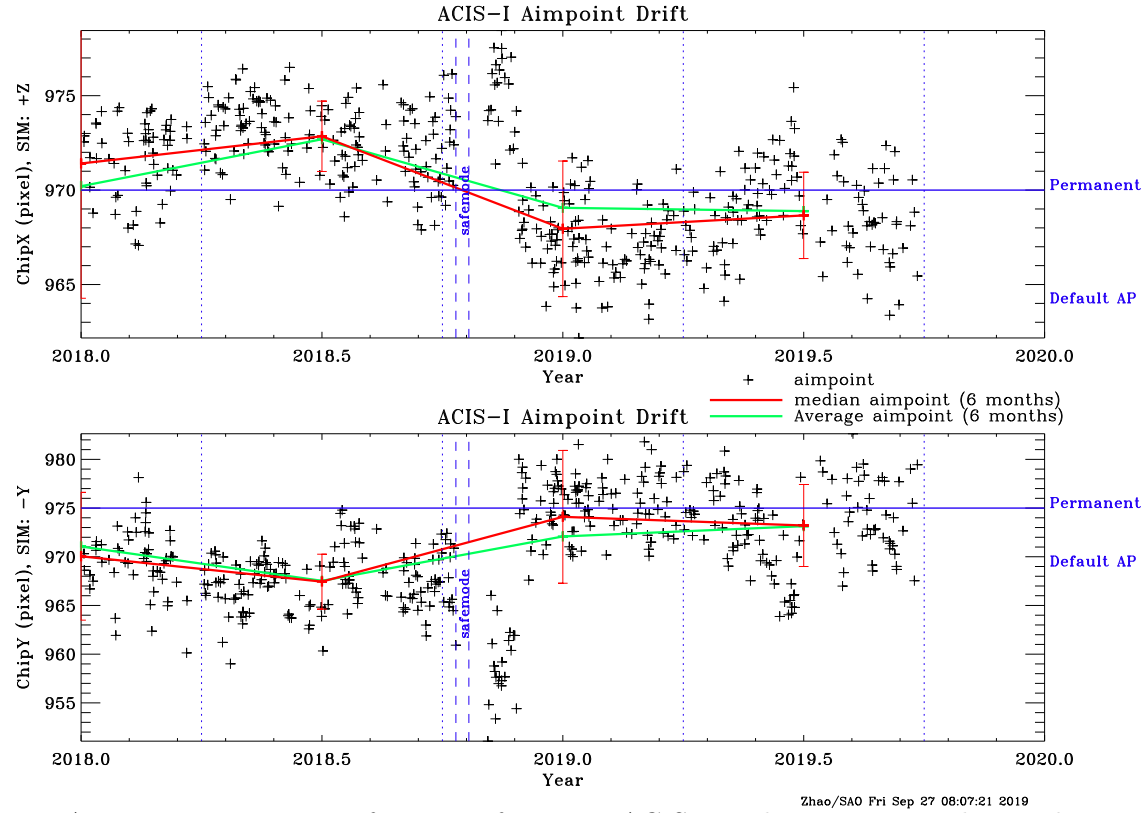

Figure 14: Aimpoint position as a function of time on ACIS-I in the past year. The gap between the two vertical dashed lines indicate when Chandra was in safemode (Oct. 10–21, 2018).

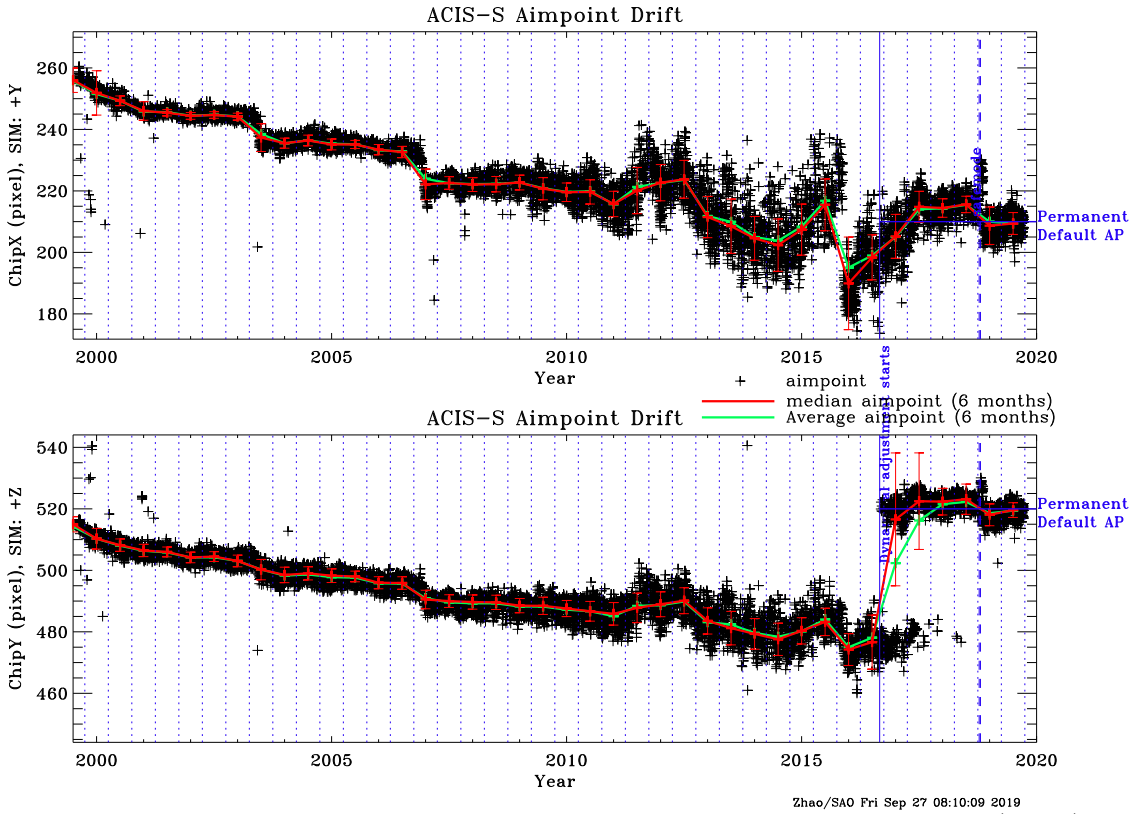

Figure 15: Aimpoint position as a function of time on ACIS-S since launch. Solid red (green) lines show the median (average) aimpoint drift in 6 month bins, separated by vertical dotted blue lines. The vertical solid blue line indicates the start of the dynamical aimpoint adjustment.

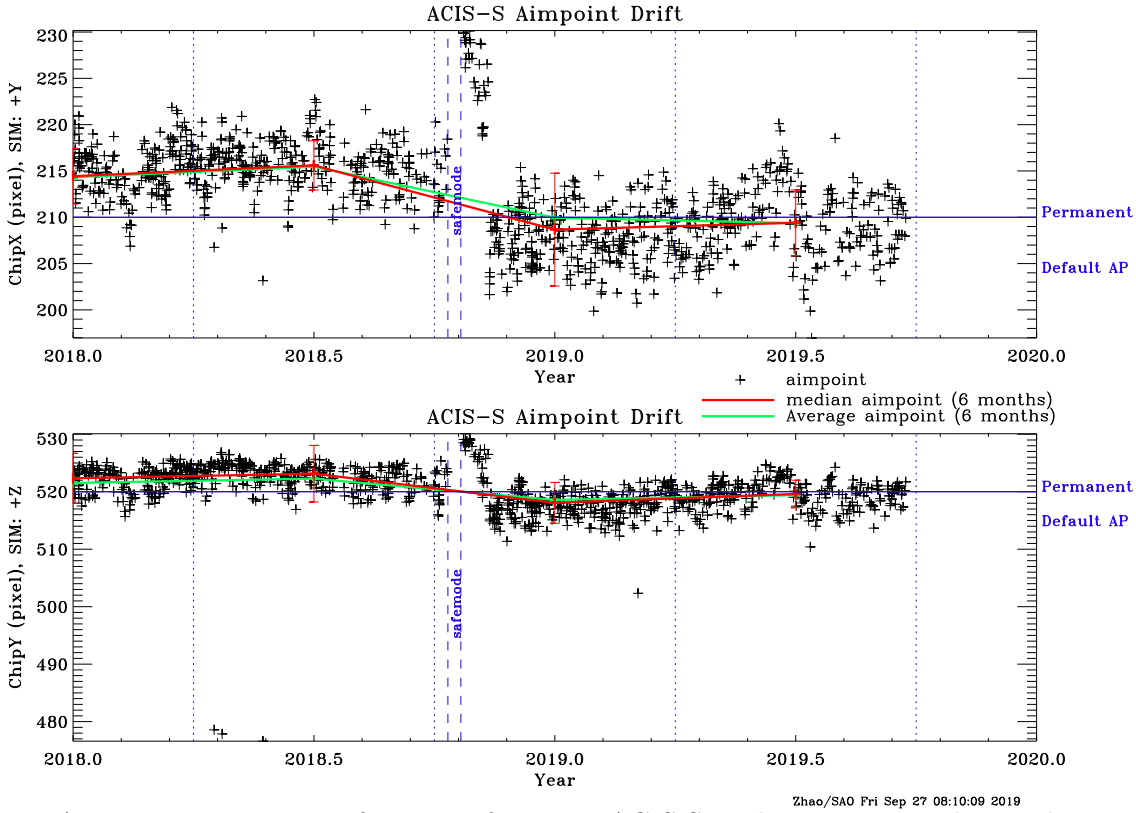

Figure 16: Aimpoint position as a function of time on ACIS-S in the past year. The gap between the two vertical dashed lines indicate when Chandra was in safemode (Oct. 10–21, 2018).

5 Optical Axis and Aimpoint on Detectors (1999 – 2015)

The optical axis positions are measured only on HRC-I as described in Section 4.1. However, at any given time, the relative position between the aimpoint and optical axis is the intrinsic property of the HRMA and ACA, independent of the detectors. One can therefore calculate the optical axis position on other detectors based on its relative position to the aimpoint.

Aimpoint positions are, however, measured on all four detectors as described in Section 4.2.

Figures 17 and 18 show the optical axis and aimpoint positions on HRC-I and HRC-S. The blue diamonds show the optical axis positions. The red arrows show the aimpoint position drift. While the optical axis is relatively stable, the aimpoint has been drifting in the SIM [−Y,−Z] direction since the Chandra launch until early 2011, for about 24″. Then it reversed its drift direction, especially after the safemode in July 2011. In early 2012, the aimpoint drift is again back to its original trend in the SIM [Y,Z] direction. Since the late 2014, the drift is reversed again. Starting on August 29, 2016 (Cycle 18), aimpoint is dynamically adjusted to put at the permanent default position (marked as red "×") near the optical axis. The dotted and dashed rectangles are the error boxes of the default aimpoint implementation, with and without the dither.

Figure 19 shows the optical axis and aimpoint positions on ACIS-I. The aimpoint positions are measured directly on ACIS-I. The optical axis positions are calculated based on their relative positions to the aimpoint from HRC-I. The green arrows in the Figure indicate the default offsets applied to avoid the on-axis target falling off the ACIS-I3 edge during the dither (see Section 6 for more details). The ACIS-I observations were conducted without default offset since launch until late 2006. Due to the aimpoint drifting, from December 2006 to December 2013, all the ACIS-I observations were conducted with a default offset of Y-offset = −15″ and Z-offset = −12″, unless the observers requested otherwise. Due to its accelerated drift since early 2012, the aimpoint was once again very close to the upper edge of the ACIS-I3 in late 2013. So since December 2013, a new default offset of Y-offset = −18″ and Z-offset = −18″ was applied, until the permanent default aimpoint (marked as red "×") was implemented in Cycle 18. The dotted and dashed rectangles are the error boxes, with and without the dither.

Figure 20 shows the optical axis and aimpoint positions on ACIS-S. The aimpoint positions are measured directly on ACIS-S. The optical axis positions are calculated based on their relative positions to the aimpoint from HRC-I. Because of the aimpoint drift, four different default offsets have been implemented between August 1999 and August 2011, in order to avoid the dither pattern falling on the node boundary 0|1. These are indicated by the green arrows in the figure (see Section 6 for more details). Due to its accelerated drift since early 2012, the aimpoint moved far enough from the node boundary 0|1. So since December 2013, a fifth default offset of Y-offset = 0″ and Z-offset = −18″ was applied, to move the aimpoint closer to the optical axis, until the permanent default aimpoint (marked as red "×") was implemented in Cycle 18. The dotted and dashed rectangles are the error boxes, with and without the dither.

Figure 21 shows the four figures the same as Figures 17 – 20 and with colored ovals indicating the 1-σ error ellipse for data in a given half year bin.

Figure 22 is the same as Figure 21 and with colored dots showing the aimpoints of individual observations.

Figure 23 shows the four figures the same as Figures 17 – 20, but with the same SIM coordinate orientation (SIM-Z up, SIM-Y right, refer Figure 2). It shows the relative positions of the optical axis (blue) and the the aimpoint (red). It also shows the aimpoints drifted in the same direction on the four detectors.

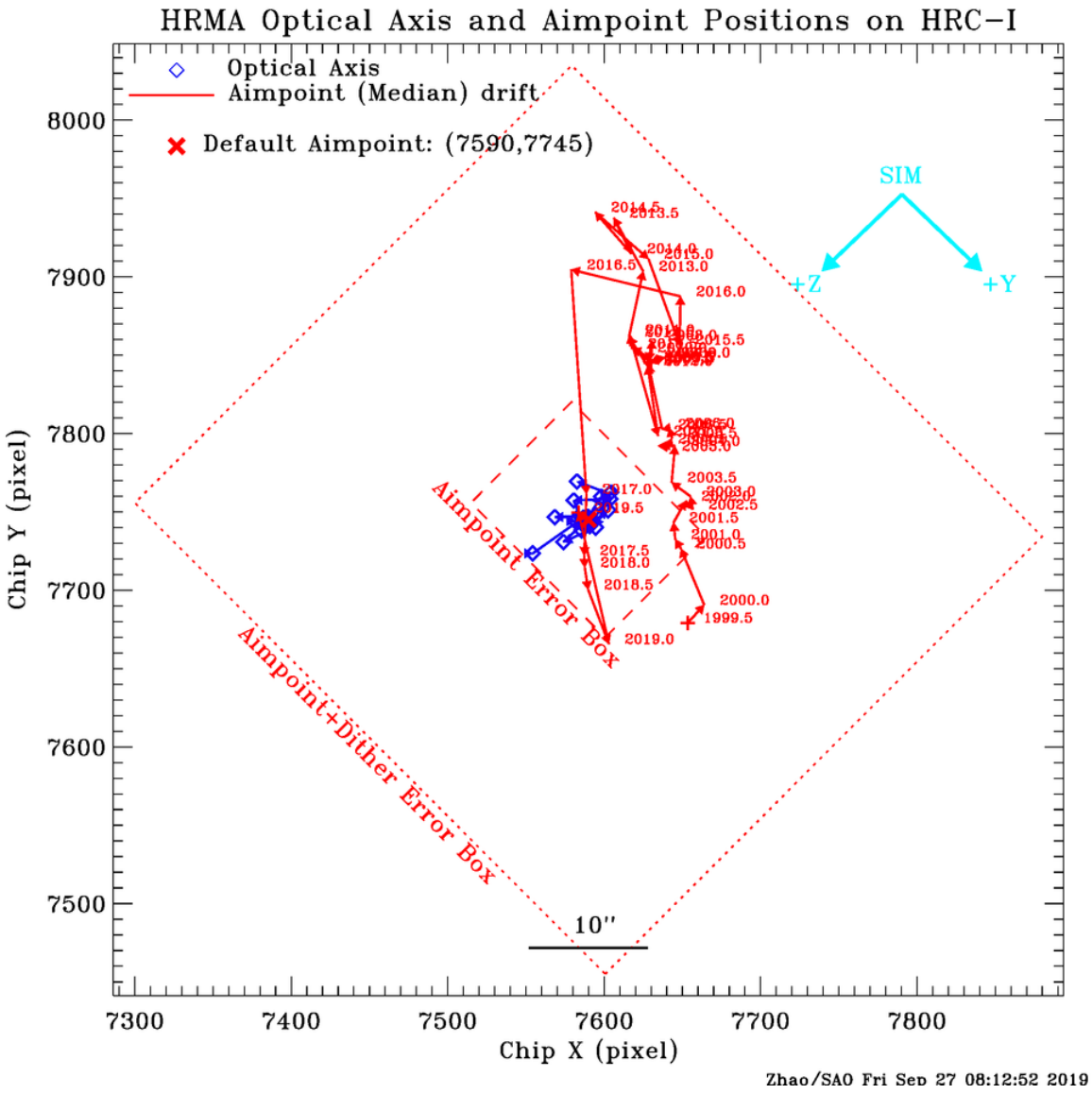

Figure 17: Chandra optical axis (blue) and median aimpoint (red, see Fig. 9) positions in half year bins on HRC-I. Each aimpoint position is labeled by the year. Starting in 2016 (Cycle 18), aimpoint is dynamically adjusted to put at the permanent default position (marked as red "×") near the optical axis. The dotted and dashed rectangles are the error boxes of the default aimpoint implementation, with and without the dither. The cyan colored arrows show the SIM coordinates.

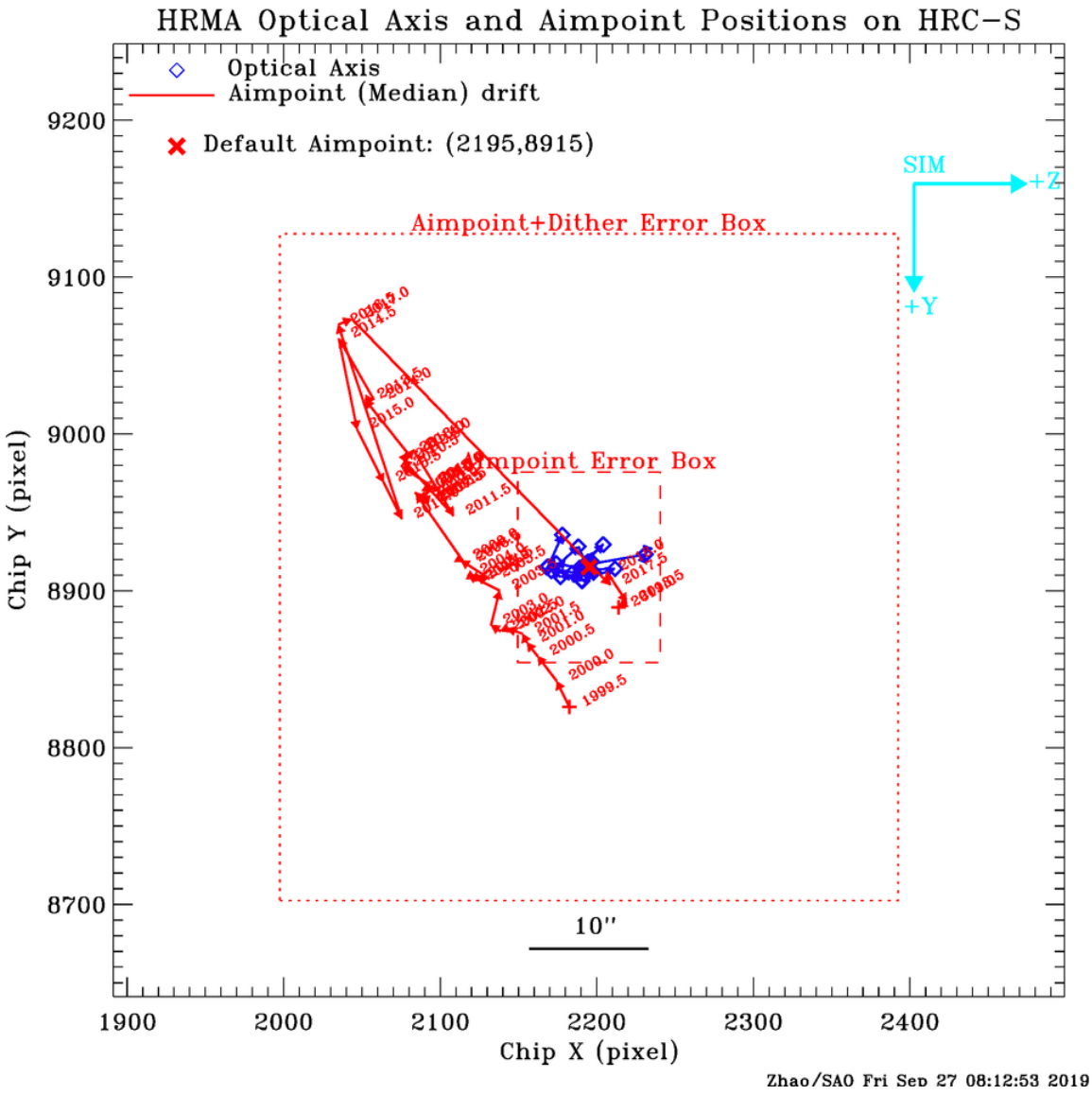

Figure 18: Chandra optical axis (blue) and median aimpoint (red, see Fig. 11) positions in half year bins on HRC-S. Each aimpoint position is labeled by the year. Starting in 2016 (Cycle 18), aimpoint is dynamically adjusted to put at the permanent default position (marked as red "×") near the optical axis. The dotted and dashed rectangles are the error boxes of the default aimpoint implementation, with and without the dither. The cyan colored arrows show the SIM coordinates.

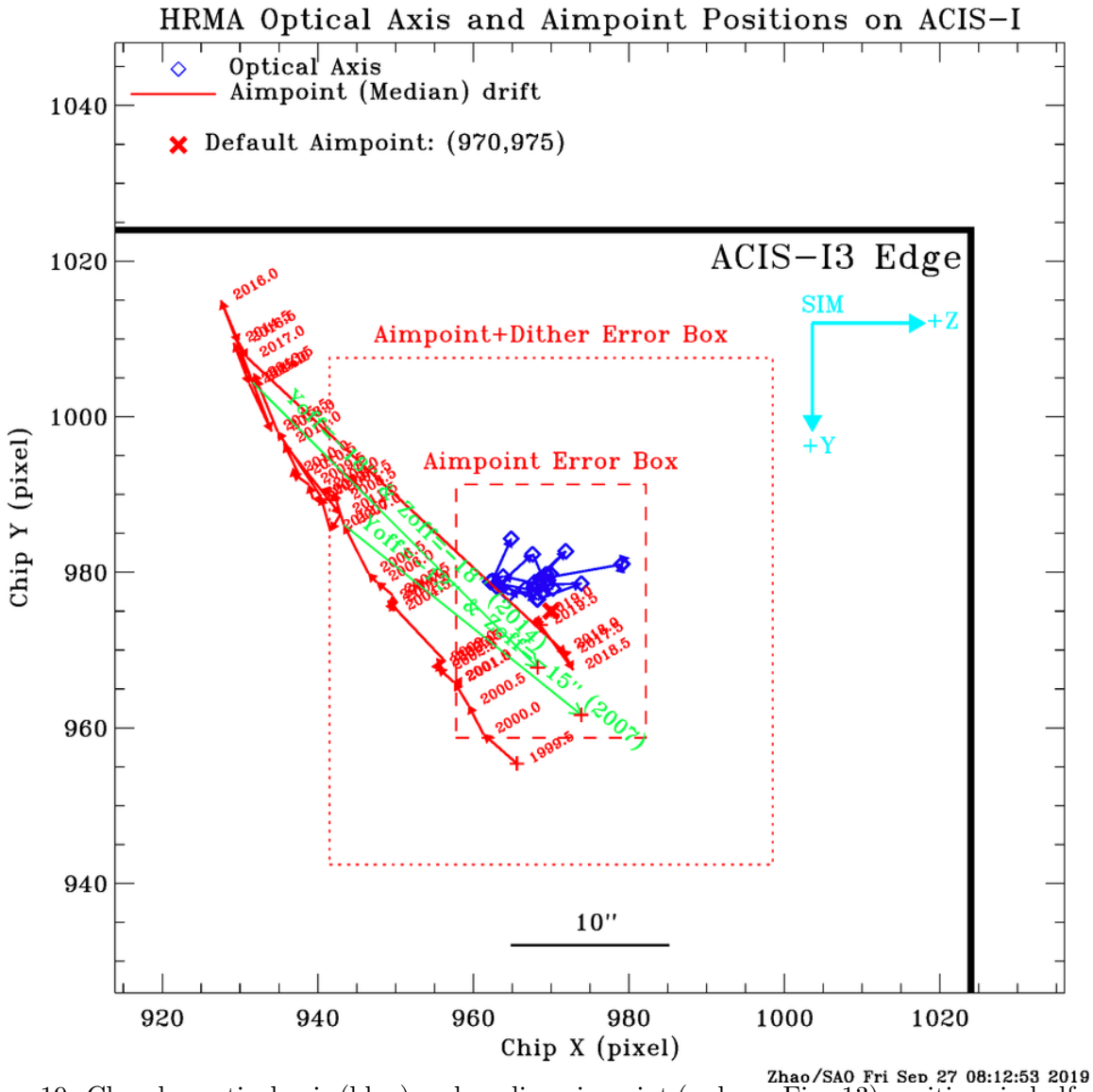

Figure 19: Chandra optical axis (blue) and median aimpoint (red, see Fig. 13) positions in half year bins on ACIS-I. Each aimpoint position is labeled by the year. The green arrows in the figure show the default offsets (starting in the year labels next to the green arrows) applied before 2016. All the observations were conducted with these default offsets, unless the observers requested otherwise. Starting in 2016 (Cycle 18), aimpoint is dynamically adjusted to put at the permanent default position (marked as red "×") near the optical axis. The dotted and dashed rectangles are the error boxes of the default aimpoint implementation, with and without the dither. The cyan colored arrows show the SIM coordinates.

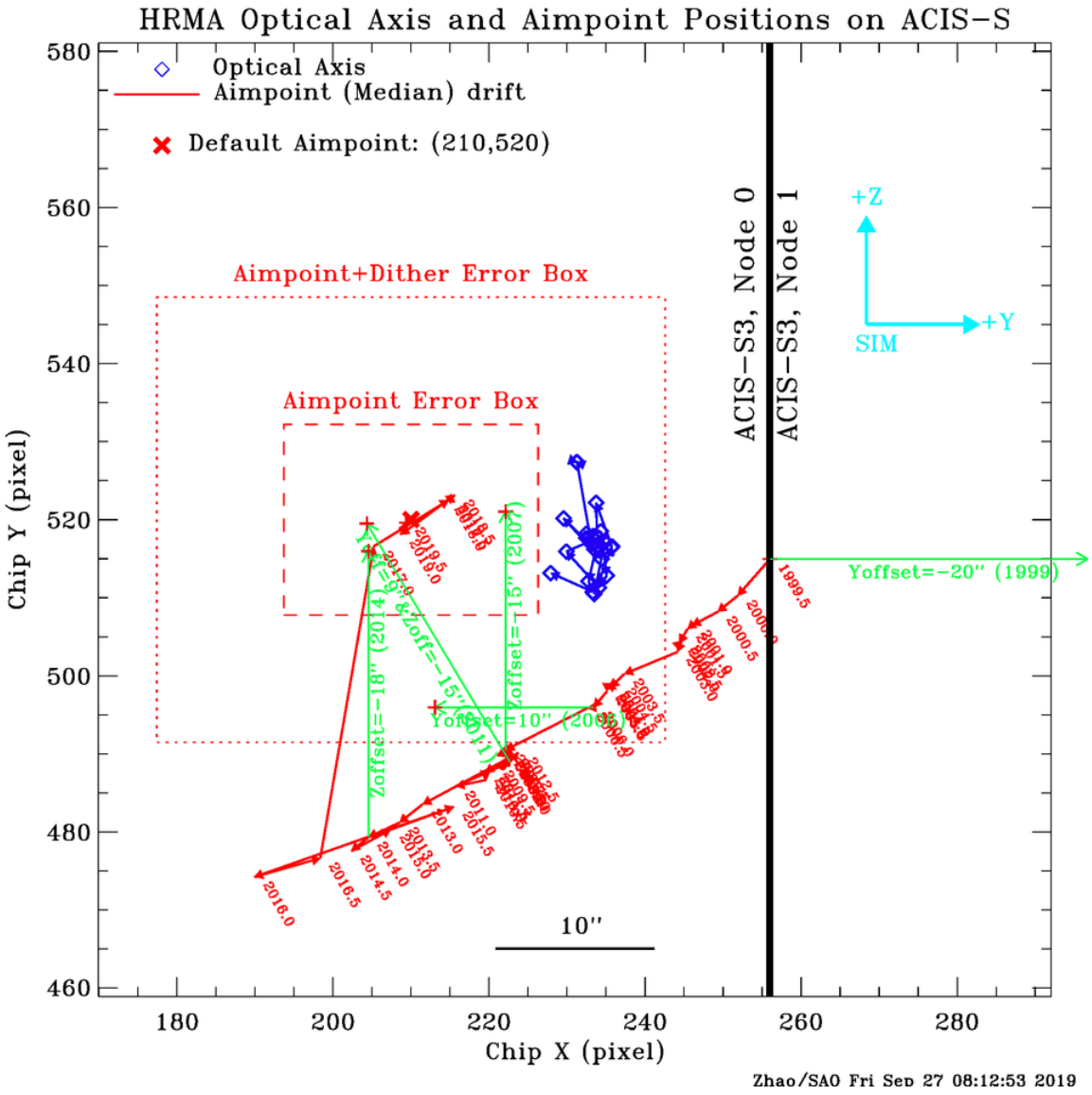

Figure 20: Chandra optical axis (blue) and median aimpoint (red, see Fig. 15) positions in half year bins on ACIS-S. Each aimpoint position is labeled by the year. The green arrows in the figure show the default offsets (starting in the year labels next to the green arrows) applied before 2016. All the observations were conducted with these default offsets, unless the observers requested otherwise. Starting in 2016 (Cycle 18), aimpoint is dynamically adjusted to put at the permanent default position (marked as red "×") near the optical axis. The dotted and dashed rectangles are the error boxes of the default aimpoint implementation, with and without the dither. The cyan colored arrows show the SIM coordinates.

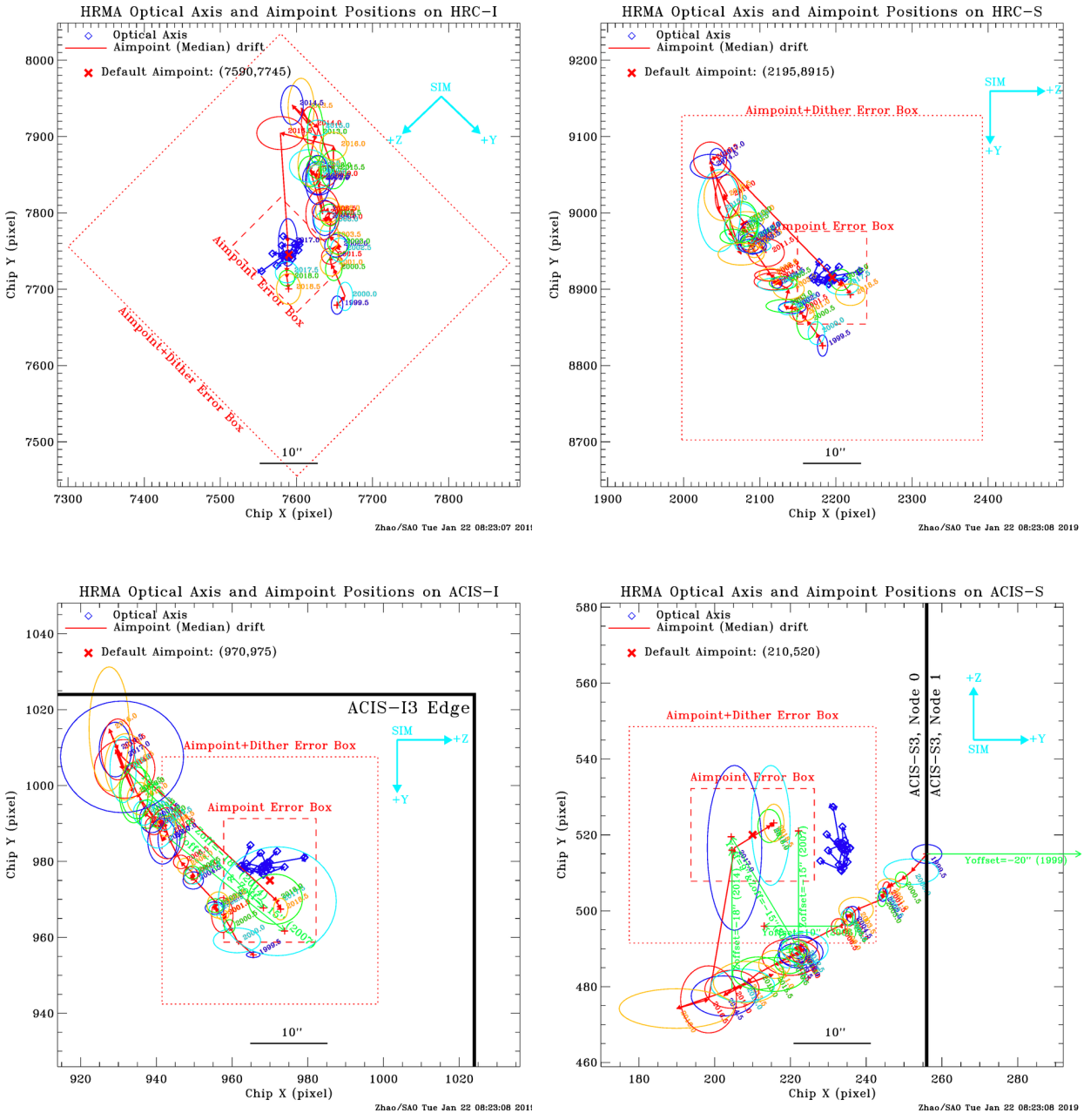

Figure 21: Same as Figures 17 – 20, the optical axis (blue) and median aimpoint (red) drifts on HRC-I (upper-left), HRC-S (upper-right), ACIS-I (lower-left) and ACIS-S (lower-right), with the colored ovals indicating the 1-σ error ellipse for data in a given half year bin.

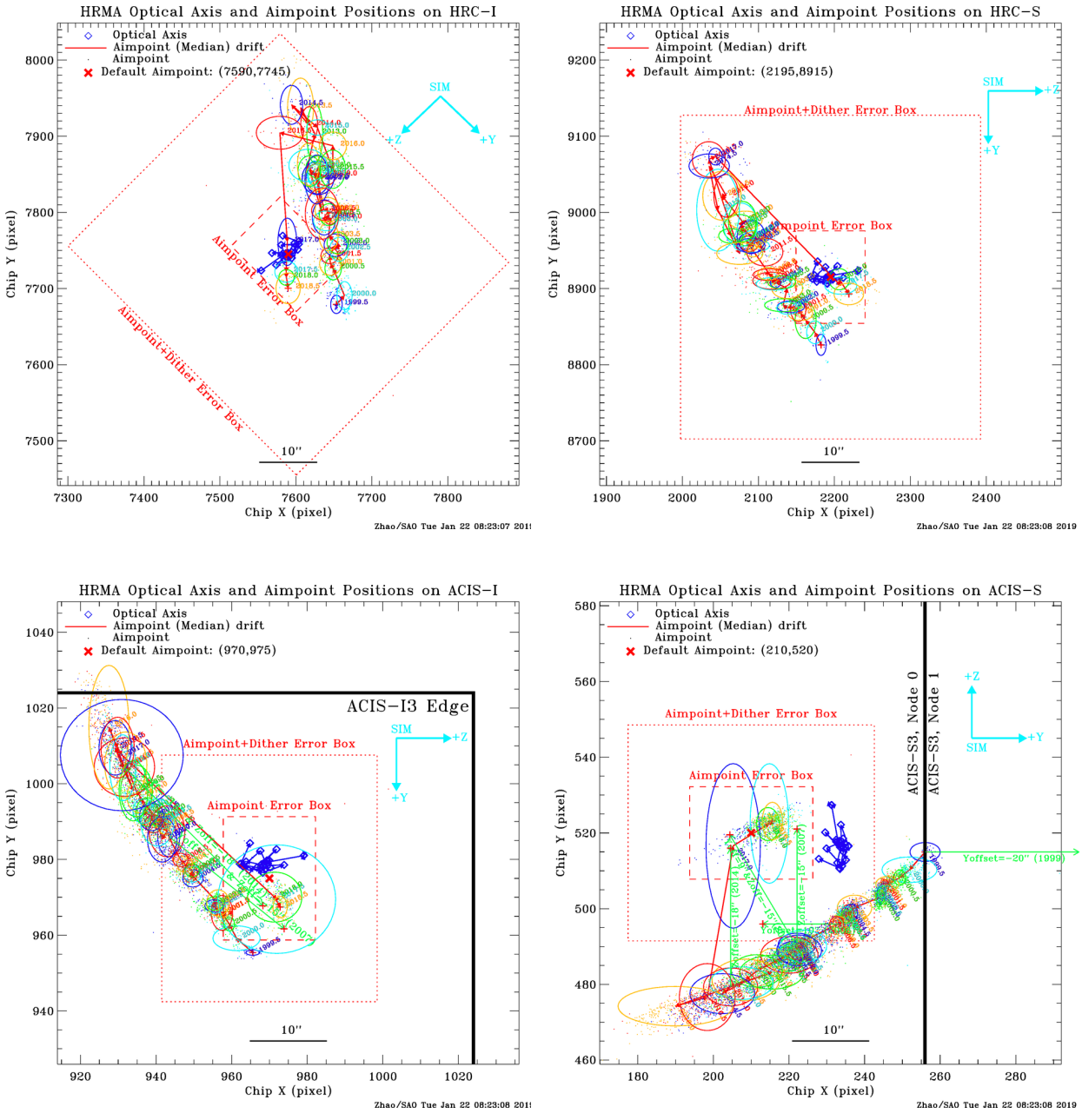

Figure 22: Same as Figures 21, the dots near the ovals of the same color are the aimpoints of individual observations for that given half year.

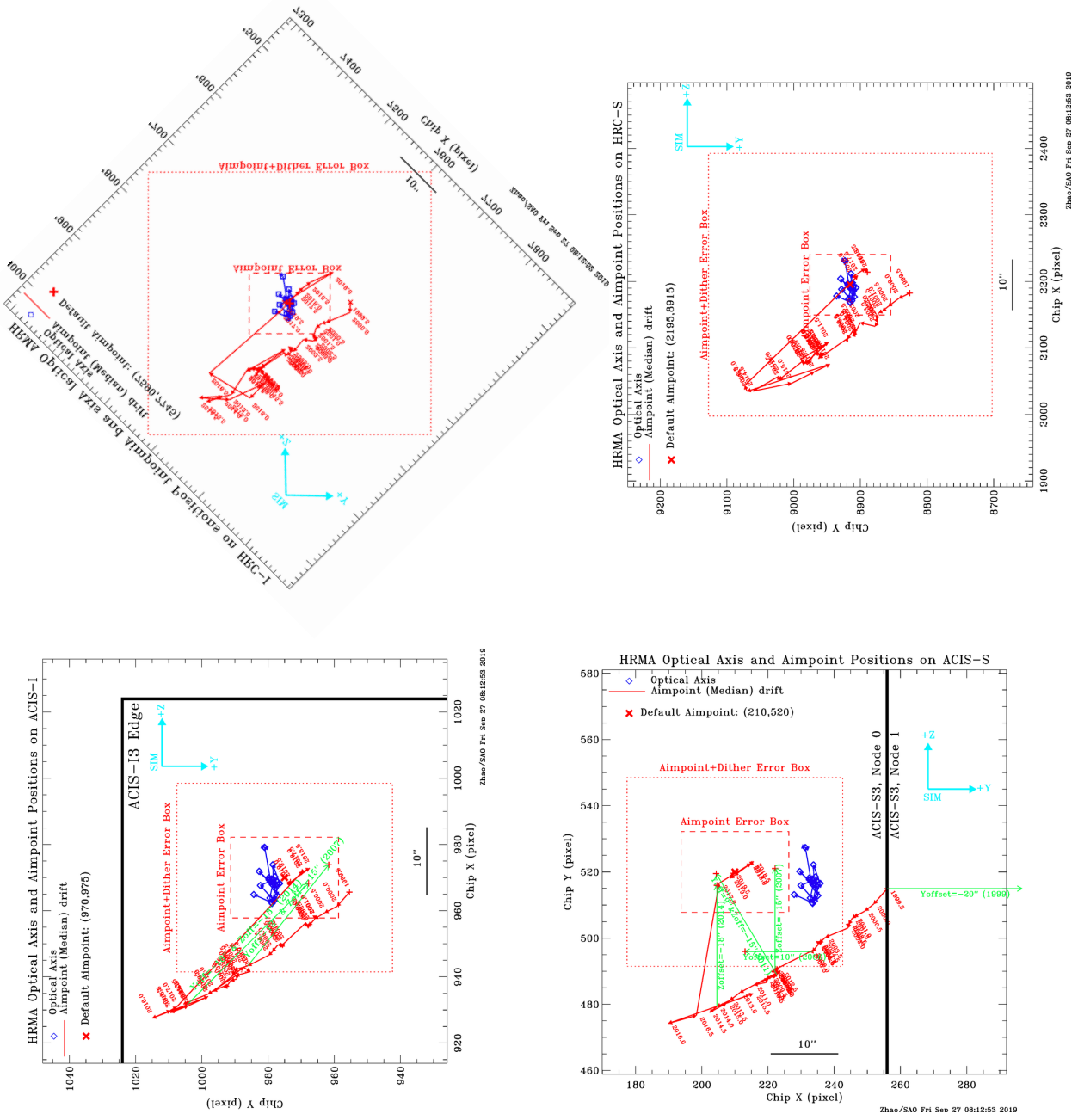

Figure 23: Same as Figures 17 – 20, but with the same SIM coordinate orientation (SIM-Z up, SIM-Y right, refer Figure 2). The aimpoints (red) drift in the same direction on HRC-I (upper-left), HRC-S (upper-right), ACIS-I (lower-left) and ACIS-S (lower-right).

6 Aimpoint Default Offsets (1999 – 2015)

It is not desirable for the aimpoint to be too close to the edge of an ACIS chip or node boundary. Before 2016, in order to avoid the dithered image of on-axis targets falling off the edge or crossing the node boundary, default pointing offsets were applied on ACIS detectors. Since the aimpoint has been drifting, the default offset has been adjusted accordingly during the course of the Chandra operation. Table 1 summarizes these default offset implementations on ACIS-I and ACIS-S since the Chandra launch. They are illustrated in Figures 19 and 20 with green arrows.

Table 1: Default Offsets from Aimpoint on ACIS Detectors

Detector	Date Applied	Y-offset	Z-offset	Reason
ACIS-I	1999 Aug.	$0''$	$0''$	No offset needed.
	2006 Dec.	$-12''$	$-15''$	Move the aimpoint away from the I3 edge & closer to optical axis.
	2013 Dec.	$-18''$	$-18''$	Move the aimpoint away from the I3 edge & closer to optical axis.
ACIS-S	1999 Aug.	$-20''$	$0''$	Move the aimpoint away from node 0|1
	2005 Dec.	$+10''$	$0''$	Move the aimpoint away from node 0|1
	2006 Dec.	$0''$	$-15''$	Move the aimpoint closer to optical axis.
	2011 Aug.	$+9''$	$-15''$	Move the aimpoint away from node 0|1 & closer to the optical axis.
	2013 Dec.	$0''$	$-18''$	Move the aimpoint closer to optical axis.

The aimpoints on HRC-I and HRC-S are well within the center regions of both detectors. Thus there were no default offset ever needed for HRC detectors.

7 Impact on Chandra Observations (1999 – 2015)

Because the optical axis position has been relatively stable (as shown in Section 4.1), the HRMA PSF and therefore the superb Chandra imaging resolution has always been the same since the Chandra launch.

Given the aimpoint has been drifting and appropriate default offsets have been implemented to compensate the drift (see Section 6), the relative positions of the optical axis and aimpoint has been changing, but at no time they were more than $27''$ apart. Since this is relatively small comparing to the offaxis angle at which the PSF starting to degrade (See POG Figures 4.12 and 4.13), the PSF of near axis sources has always stayed the same during the entire Chandra operation.

8 Permanent Default Aimpoints (2016 –)

As stated in Section Section 4.2, starting with Cycle 18 observations, a permanent default aimpoint is chosen for each detector to mitigate the effect of the aimpoint drifting. These permanent default aimpoints are close enough to the optical axis so the PSFs are as sharp as on the optical axis, while also far from the chip edges or node boundaries. At the same time, a dynamical aimpoint adjustment process are implemented to put the on-axis coordinate at the permanent default aimpoints.

The dynamical aimpoint adjustment started on August 29, 2016. The adjustment is based on a thermal model to predict the ACA housing temperaturefor each observation and then calculate

the expected alignment offsets based on that temperature. Those offsets are then applied to the PCAD/ACA attitude for that observation. This process has improved the aimpoint stability. If the observers do not choose any offset, the best effort will be made to put the on-axis target on the default aimpoint. However, due to the unpredictability of the thermal changes in the ACA, error boxes are given around each aimpoint, indicating the current pointing uncertainty. The error boxes for the permanent default aimpoints are based on the observations taken on all the detectors during the 6 month period prior to November 2019. The peak to peak swings of the short term fluctuations are 13″ in the SIM +Y direction and 7″ in the SIM +Z direction. They are improved from last year's 16″ in the SIM +Y direction and 12″ in the SIM +Z direction. However, we want to continue to monitor the aimpoint positions to see if the improvement is stable. So we would like to keep last year's error boxes to be conservative. In addition, the ACIS observations have a dither of 16″ amplitude, and the HRC observations have a dither of 40″ amplitude. So the error boxes are the same as last year: For ACIS, $16'' \times 12''$ and $56'' \times 52''$ including the dither.

Observers also have the option to request the Y-offset, Z-offset and SIM-Z offset (the same as previous cycles) to put their targets at different locations on the detector. These offsets will be calculated from the default aimpoint. Observers can use *ObsVis* to visualize the target location on the detectors with their chosen offsets. However, the error boxes will be the same size around their chosen location.

9 Optical Axis and Permanent Default Aimpoint positions

The current optical axis with their standard deviation (σ), and the permanent default aimpoint with their error boxes are listed in Table 2. These numbers are used in *CIAO* (Chandra Interactive Analysis of Observations) and *ObsVis* (The Chandra Observation Visualizer).

On-axis targets will be imaged near the aimpoint and inside the error box on each detector. Observers should use this table to check their target location and may request different pointing offset based on their sources to maximize the scientific return. If the observer does not request a specific pointing offset, their on-axis coordinates will be put near the default aimpoint. Table 2 can also be found at `http://cxc.harvard.edu/cal/Hrma/OpticalAxisAndAimpoint.html`.

Figures 24 – 27 show the optical axis and permanent default aimpoint with their error boxes on all four detectors.

Table 2: Chandra Optical Axis and Permanent Default Aimpoint Positions

Detector	SIM-Z (mm)	Optical Axis (pixel)		Permanent Default Aimpoint (pixel)		Error Box without dither (pixel)	Error Box with dither (pixel)	Chip
		ChipX(σ)	ChipY(σ)	ChipX	ChipY			
ACIS-I	−233.587	961.8(4.4)	977.3(4.4)	970	975	$12'' \times 16''$ (24.4×32.5)	$28'' \times 32''$ (56.9×65.0)	I3
ACIS-S	−190.143	235.0(4.4)	510.1(4.4)	210	520	$16'' \times 12''$ (32.5×24.4)	$32'' \times 28''$ (65.0×56.9)	S3
HRC-I	126.983	7609.4(22.0)	7759.3(8.0)	7590	7745	$16'' \times 12''$ (121.4×91.1) SIM [Y,Z]	$56'' \times 52''$ (425.0×394.7) SIM [Y,Z]	
HRC-S	250.466	2166.4(16.5)	8909.3(16.5)	2195	8915	$12'' \times 16''$ (91.1×121.4)	$52'' \times 56''$ (394.7×425.0)	S2

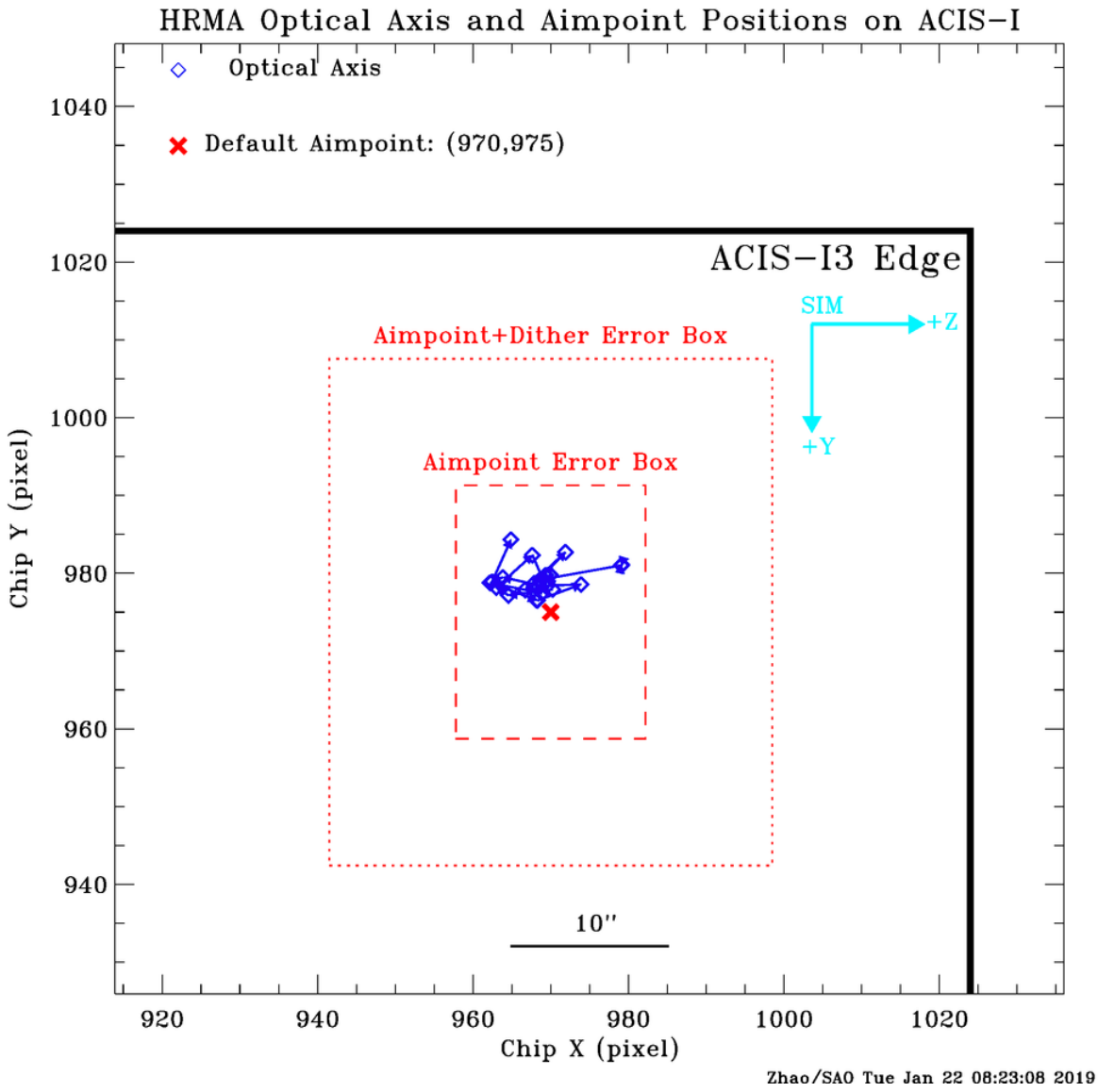

Figure 24: Chandra optical axis (blue diamonds) positions for each year and permanent default aimpoint (red cross) on ACIS-I at [970,975]. The small box (red dashed line, $12'' \times 16''$, or 24.4×32.5 pixels) centered at the aimpoint is the error box of the aimpoint center, i.e. an on-axis target can be anywhere inside this box. The large box (red doted line, $28'' \times 32''$, or 56.9×65.0 pixels) is the error box of aimpoint with dither.

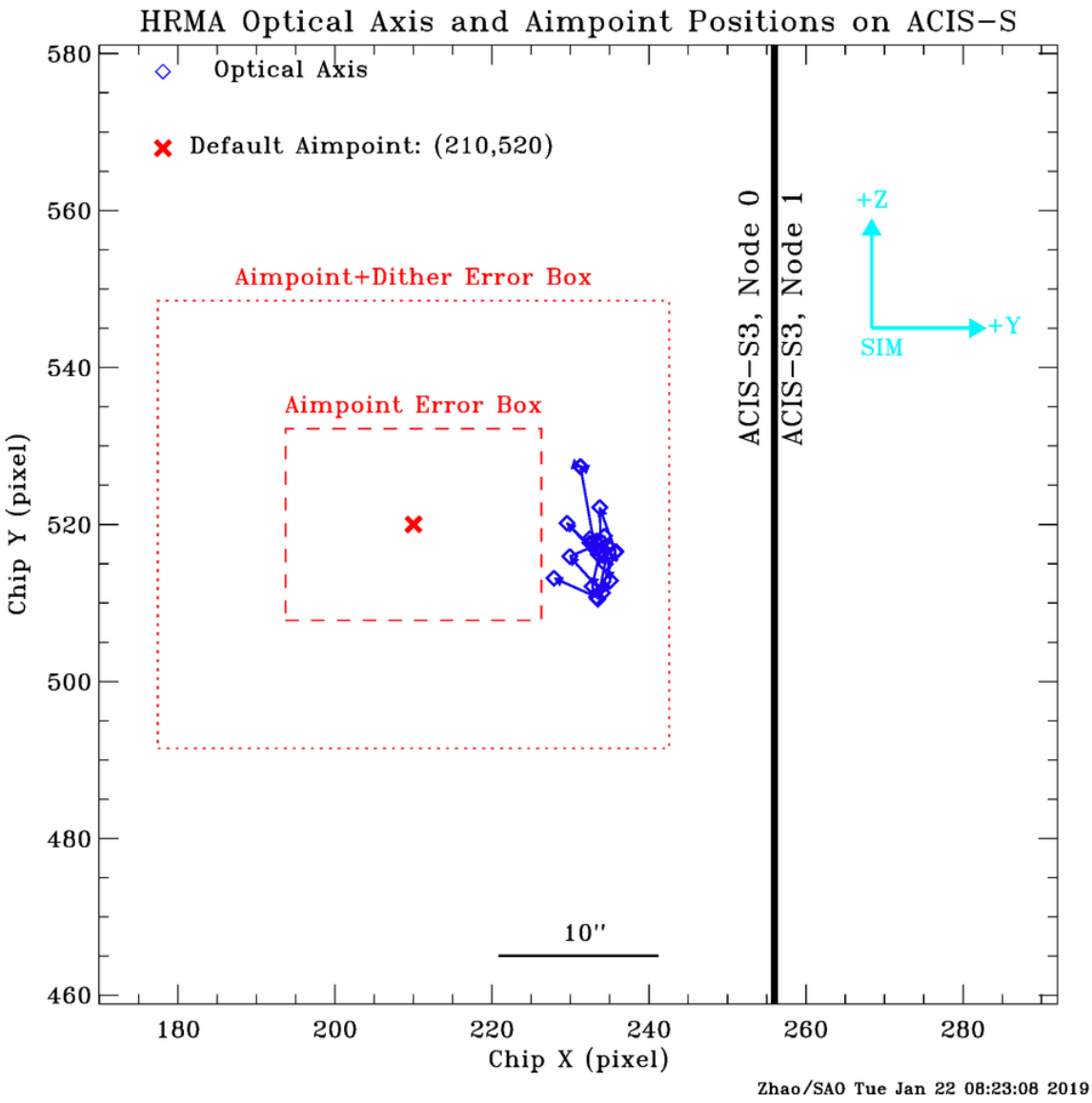

Figure 25: Chandra optical axis (blue diamonds) positions for each year and permanent default aimpoint (red cross) on ACIS-S at [210,520]. The small box (red dashed line, $16'' \times 12''$, or 32.5×24.4 pixels) centered at the aimpoint is the error box of the aimpoint center, i.e. an on-axis target can be anywhere inside this box. The large box (red doted line, $32'' \times 28''$, or 65.0×56.9 pixels) is the error box of aimpoint with dither. Note the permanent default aimpoint is $\sim 12''$ from the optical axis in order to avoid the node boundary 0|1.

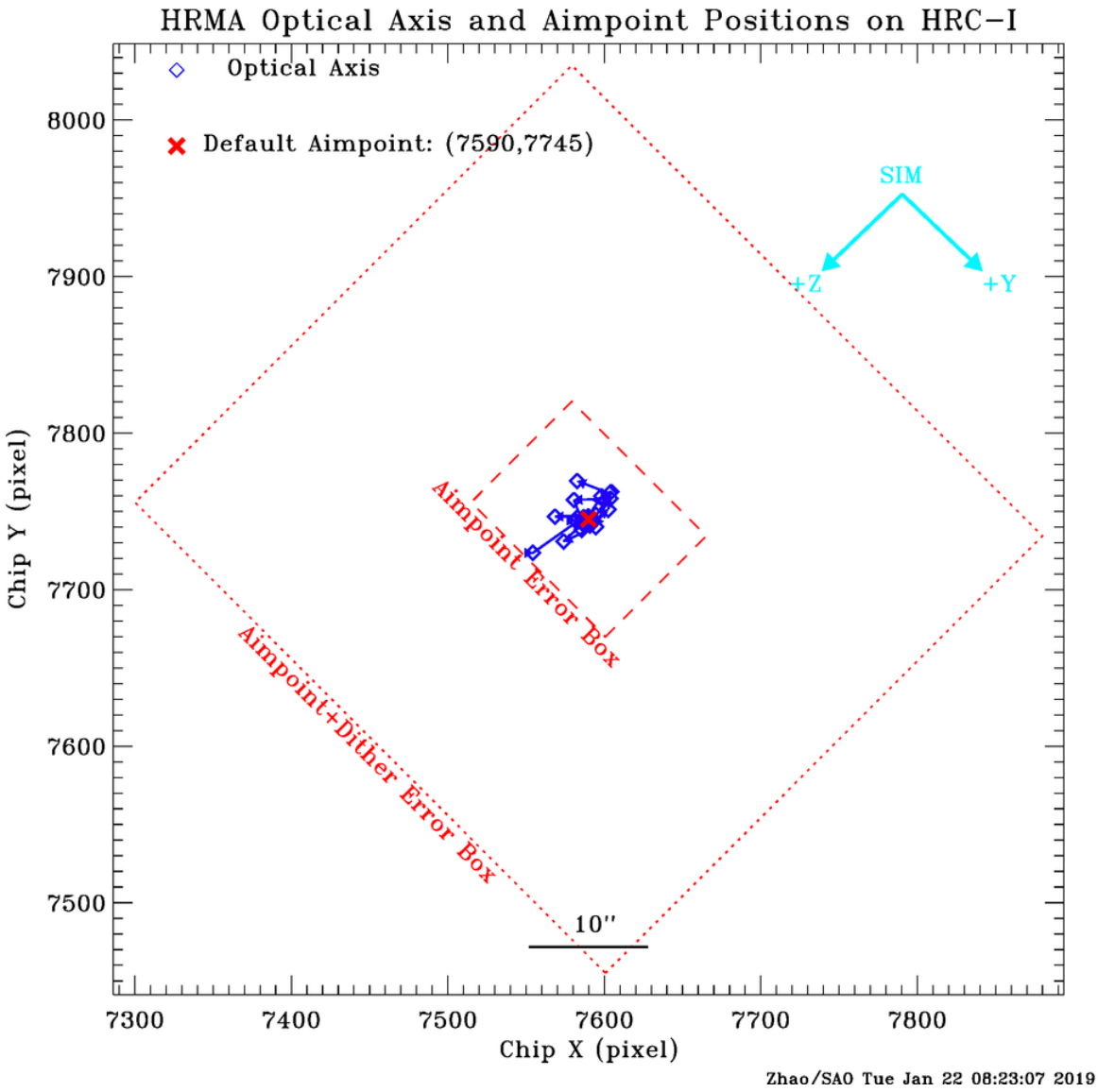

Figure 26: Chandra optical axis (blue diamonds) positions for each year and permanent default aimpoint (red cross) on HRC-I at [7590,7745]. The small box (red dashed line, $16'' \times 12''$, or 121.4×91.1 pixels in SIM [Y, Z]) centered at the aimpoint is the error box of the aimpoint center, i.e. an on-axis target can be anywhere inside this box. The large box (red doted line, $56'' \times 52''$, or 425.0×394.7 pixels in SIM [Y, Z]) is the error box of aimpoint with dither.

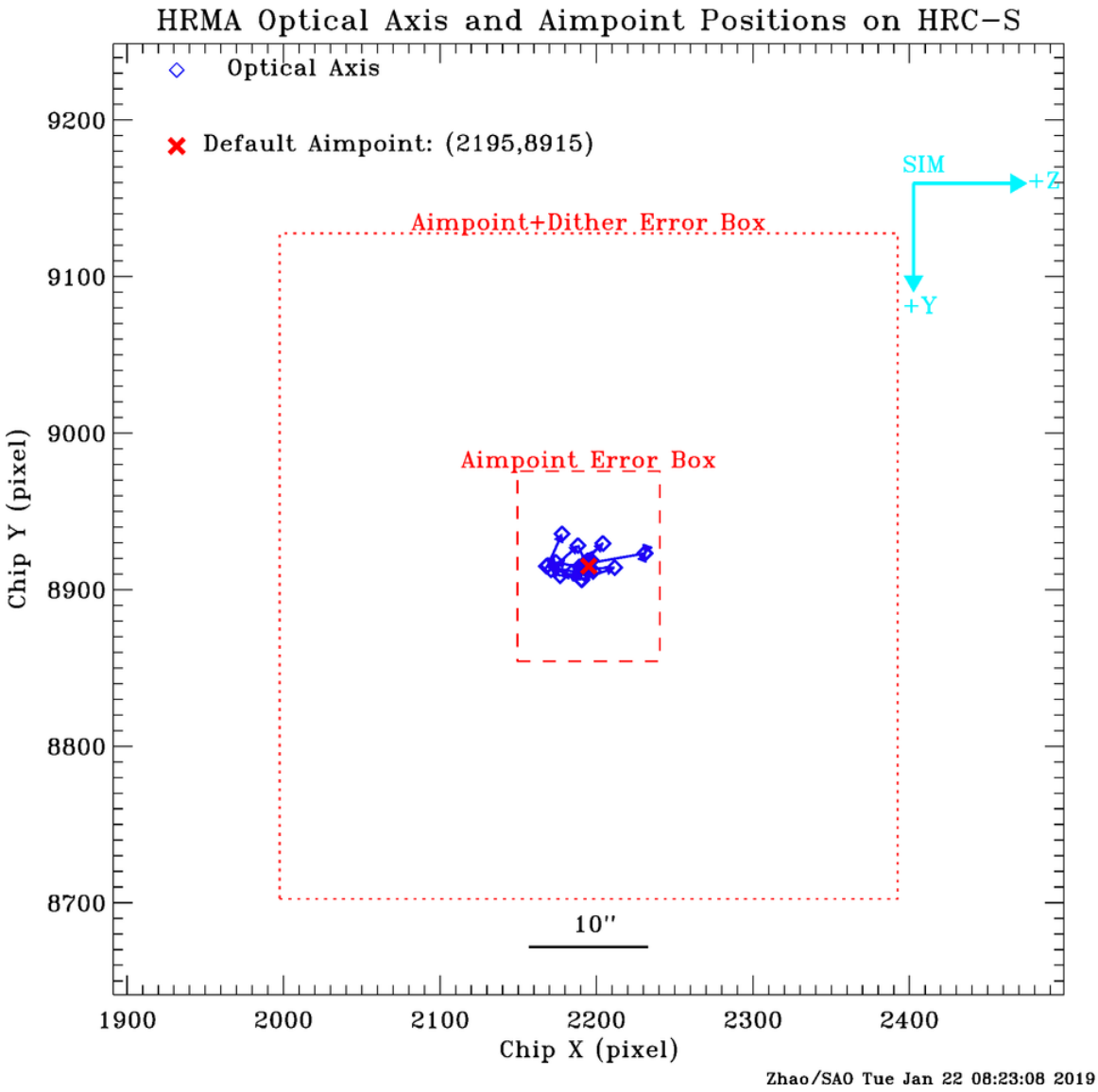

Figure 27: Chandra optical axis (blue diamonds) positions for each year and permanent default aimpoint (red cross) on HRC-S at [2195,8915]. The small box (red dashed line, $12'' \times 16''$, or 91.1×121.4 pixels) centered at the aimpoint is the error box of the aimpoint center, i.e. an on-axis target can be anywhere inside this box. The large box (red doted line, $52'' \times 56''$, or 394.7×425.0 pixels) is the error box of aimpoint with dither.

10 Summary

By studying the optical axis and aimpoint, we can understand the long term stability and imaging quality of the telescope and ensure its optimal performance.

The study shows that optical axis position has been relatively stable since the Chandra launch. Its random walk like movement is well within a 10″ region, and within a 6″ region since year 2000. The movement is consistent with the measurement errors. This result indicates that the HRMA, optical bench and SIM are all very rigid and stable. Therefore the superb Chandra spatial resolution has always been the same.

The study shows that the aimpoint has been drifting in the SIM [−Y,−Z] direction for about 30″ since launch. Since 2011 the drift has reversed its direction three times and the rate of drift has accelerated. In addition, the short term fluctuation has gradually increased. The aimpoint drift is caused by the alignment change between the ACA and the HRMA. Its long term change is due to the aging and relaxing of the material. Its short term change is usually associated with the thermal change in the ACA housing. So in order to keep the aimpoint stable in short term, we need to keep a constant temperature of the ACA.

To mitigate the accelerated drift and increased short term fluctuations, starting in Cycle 18, a permanent default aimpoint is chosen for each detector. A dynamical aimpoint adjustment process are implemented to put the on-axis coordinate at the permanent default aimpoints. The adjustment is based on a thermal model to predict the ACA housing temperature for each observation and then calculate the expected alignment offsets based on that temperature. Those offsets are then applied to the PCAD/ACA attitude for that observation.

This memorandum can be found at:
`http://cxc.harvard.edu/cal/Hrma/rsrc/Publish/Optics/OpticalAxisAndAimpoint/oxap_memo_2019.pdf`

APPENDICES

A Safemode and its Effects on Optical Axis and Aimpoint

The following passages were from the NASA's public announcement:

[Oct. 12, 2018:] "At approximately 1355 GMT on October 10, 2018, NASAs Chandra X-ray Observatory entered Safe Mode, where the telescopes instruments are put into a safe configuration, critical hardware is swapped to back-up units, the spacecraft points so that the solar panels get maximum sunlight, and the mirrors point away from the Sun. Analysis of available data indicates the transition to safe mode was nominal, i.e., consistent with normal behavior for such an event. All systems functioned as expected and the scientific instruments are safe."

[Oct. 15 Update:] "The cause of Chandra's safe mode on October 10 has now been understood and the Operations team has successfully returned the spacecraft to its normal pointing mode. The safe mode was caused by a glitch in one of Chandra's gyroscopes resulting in a 3-second period of bad data that in turn led the on-board computer to calculate an incorrect value for the spacecraft momentum. The erroneous momentum indication then triggered the safe mode."

[Oct. 24 Update:] "On the evening of October 21, Chandra returned to science observations after the team successfully carried out a procedure to enable a new gyroscope configuration for the spacecraft. The team initiated a set of maneuvers to change the pointing and orientation

of the spacecraft to confirm that the gyroscopes were behaving as expected. During the coming week, scientists will collect spacecraft data to fine-tune the performance for the new gyroscope configuration. As a final step, the team will uplink a software patch to apply any necessary adjustments to the on-board computer."

During the safemode, the HRMA mirror cavity temperature was warmed up to as high as 75°F, from the nominal of 70°F. Immediately after the safemode, the HRMA temperature was still at ~ 72°F. Then the temperature continued to cool down to its nominal value of 70°F. The operation was resumed during the HRMA cool down. The first thing done during the cool down was a series HRC-I observations of HR1099, a RS CVn binary star, to check if the safemode affected the Chandra aimpoint and optical axis. It was found that the aimpoint jumped about +6.5 aresec in SIM-Y and +3.0 aresec in SIM-Z directions after the safemode (see Figures 10, 12, 14 and 16). This could be due to the temperature warm up. This jump had direct effect for ACIS-S, as it moved the aimpoint very close to the chip S3 node 0|1 boundary. Adjustment was immediately implemented to bring the ACIS-S aimpoint away from the S3 node 0|1 boundary. After the HRMA temperature returned to normal, the aimpoints on all four detectors were again back to their default positions (see Figures 10, 12, 14 and 16).

The optical axis position was measured using the HRC-I with a simple annular scan observation of HR1099, as shown in Figures 28 and 29. The two sets of measurements were done in about 18 hours apart. The first set was done in early Oct. 22, 2018 and the second set was done in late Oct. 23, 2018. However, data from simple scans like this little cross can not be fit to the 2-D quadratic function (Eq. 1) to definitively determine the optical axis position. Because there were no confinements alone the 45° off the two orthogonal directions, a 2-D quadratic function will find minimums in multiple places alone the 45° line. To solve this problem, the following two 1-D quadratic functions were used to fit the data.

$$r_x = ax^2 + bx + c \tag{2}$$
$$r_y = dy^2 + ey + f \tag{3}$$

where x and y are the chip coordinates [X, Y]; r_x and r_y are the encircled energy radii as functions of x and y, respectively; a, b, c, d, e, f are the fitting constants.

Plugin all the x and y from the scan data separately into the two equations,. we can find the minimums of the two equations ($r_{x_{min}} = r_{x_0}(x_0)$) and ($r_{y_{min}} = r_{y_0}(y_0)$) at the chip position (x_0, y_0), which is the optical axis position.

Figure 30 shows the Chandra optical axis positions measured this way on HRC-I during the HRMA cool down with all the measurements since launch. The two measurements (2018-10a) and (2018-10b) were made on Oct. 22 and 23, 2018, respectively. They are very close to each other ($\sim 0.3''$) and only a few arcsec away from all the previous measurements.

In conclusion, the safemode of October 2018 caused the HRMA temperature to rise, which in turn caused the aimpoint to jump about +6.5 aresec in SIM-Y and +3.0 aresec in SIM-Z immediately after. The aimpoints has returned to its default positions on all detectors after the HRMA temperature returned to normal. The optical axis was measured during the HRMA cool down. Its position is a few arcsecond from the previously measured positions, which is not a significant shift. So both aimpoint and optical axis remain the same as before the safemode.

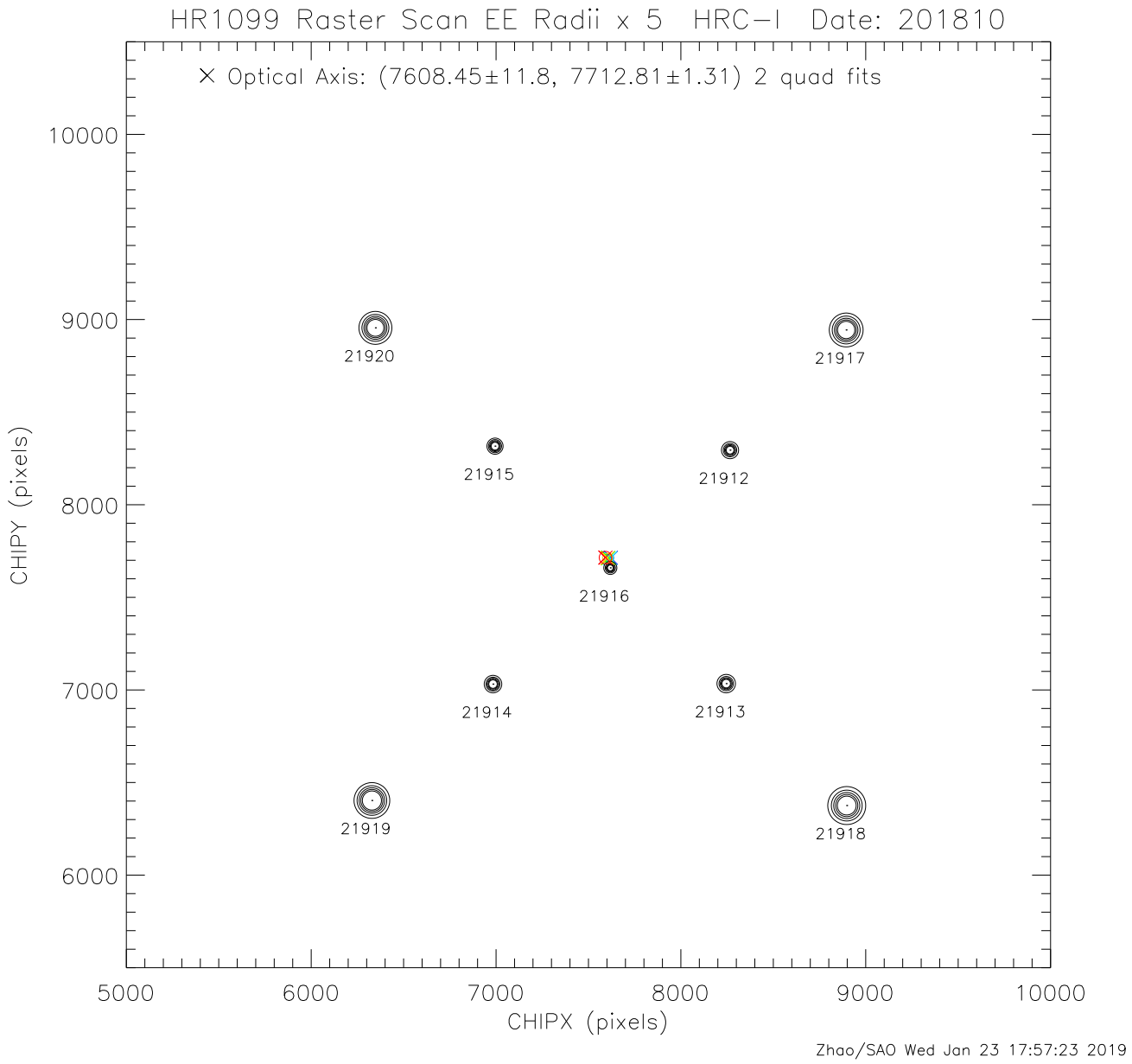

Figure 28: The first HRC-I annular scan observation of HR1099 during the HRMA cool down (in the morning of 2018-10-22). Circles around each observation point have the 50% – 90% encircled energy radii × 5. The numbers under the circles are the OBSIDs of the observations. The data are fit to two orthogonal 1-D quadratic equations. The optical axis is at the intersection of two minimum coordinates.

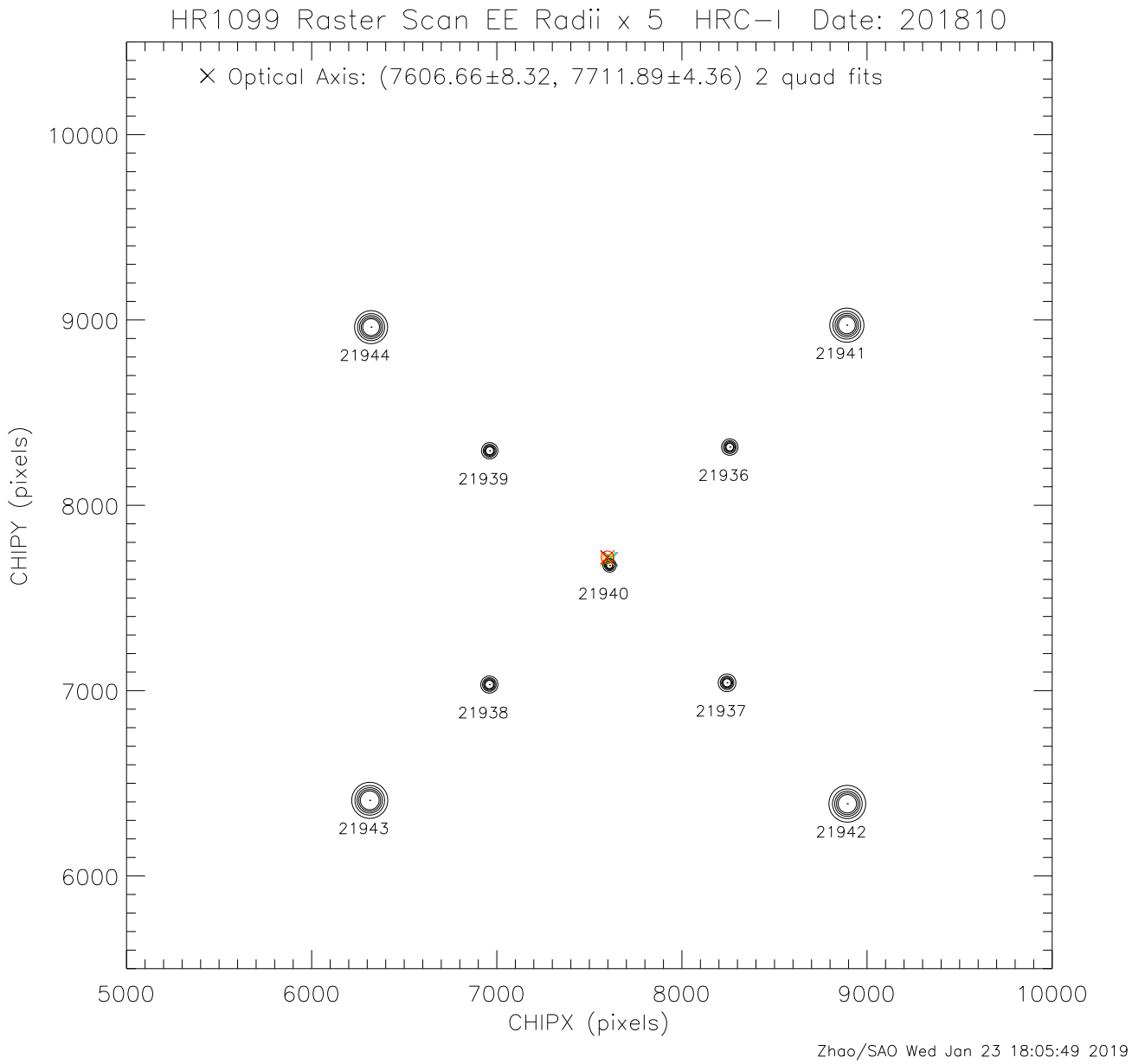

Figure 29: The second HRC-I annular scan observation of HR1099 during the HRMA cool down (taken 18 hours after the first scan, in the evening of 2018-10-23). Circles around each observation point have the 50% – 90% encircled energy radii × 5. The numbers under the circles are the OBSIDs of the observations. The data are fit to two orthogonal 1-D quadratic equations. The optical axis is at the intersection of two minimum coordinates.

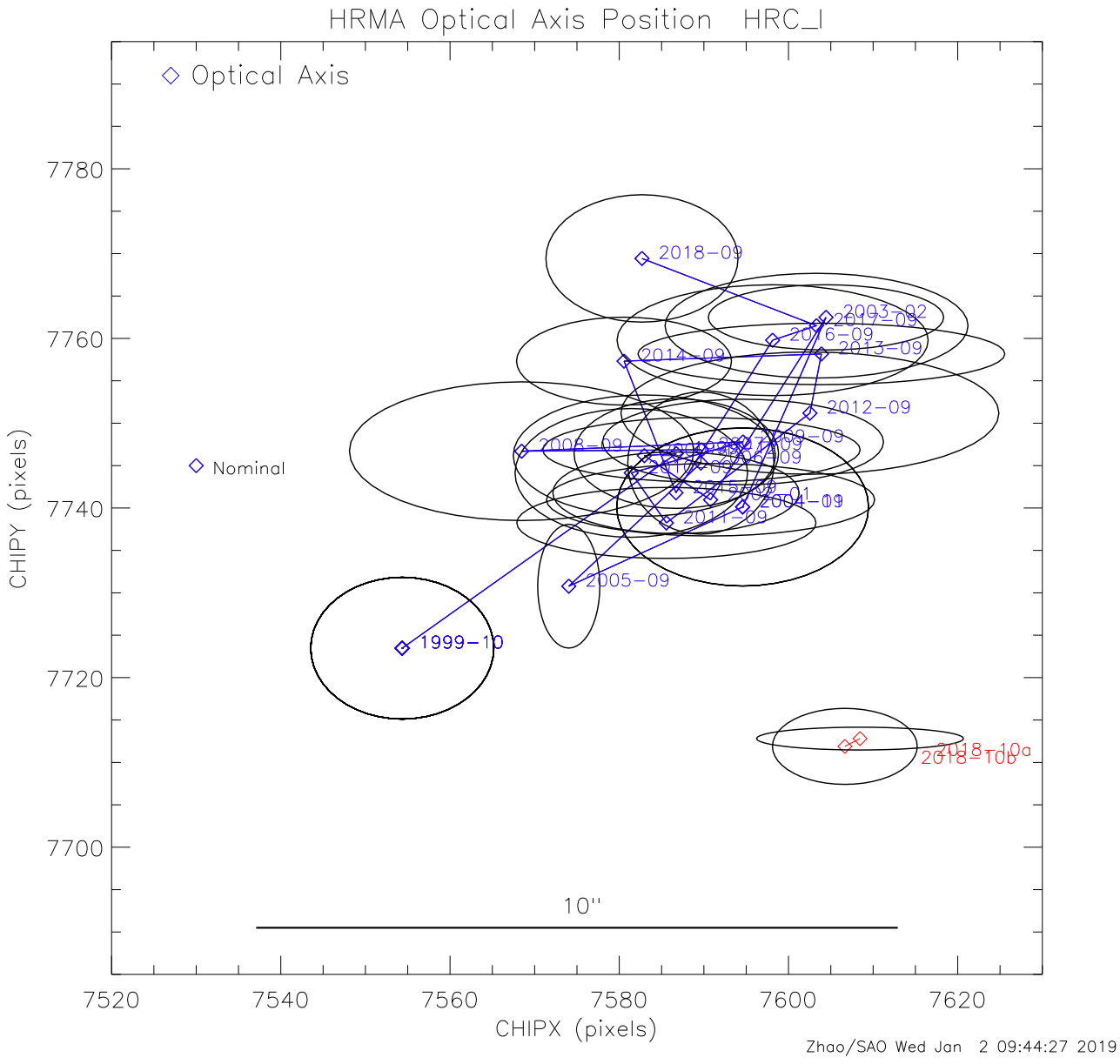

Figure 30: Chandra optical axis positions measured on HRC-I during the HRMA cool down after the safemode 2018 (red diamonds) with all the measurements since launch (blue diamonds). Each position is labeled by the year–month. The ellipse around each position is the $1-\sigma$ measurement error ellipse for that given year. The two measurements (2018-10a) and (2018-10b) were made on Oct. 22 and 23, 2018, respectively. They are very close to each other ($\sim 0.3''$) and only a few arcsec away from all the previous measurements.

B New Annular Scan

To ensure more accurate optical axis measurements, we plan to move 20 of the 21 raster scan pointings of ArLac from the HRC-S to HRC-I in 2019. HRC-I is the only detector used to measure the optical acis. Raster scan points on the HRC-S have not been used for this purpose. Only one onaxis pointing will be kept on the HRC-S to measure the aimpoint and PSF. The total number of pointings and exposure time from both HRC detectors are kept the same.

Here is a summary of the current and new scans:

- Current Raster Scan (43 pointings, 55ks):
  - HRC-I: 2 on-axis (5ks) + 20 off-axis (1ks each) = 21 pointings (30ks)
  - HRC-S: 1 on-axis (5ks) + 20 off-axis (1ks each) = 21 pointings (25ks)
- New Annular Scan (43 pointings, 50ks)
  - HRC-I: 2 on-axis (5ks) + 40 off-axis (1ks each) = 42 pointings (50ks) (40 off-axis pointings at 1,2,3,4,6 arcmin offset on 8 azimuthal directions, every 45°.)
  - HRC-S: 1 on-axis (5ks)

The new annular scan is divided into two groups (alternating in radial and azimuthal positions) to keep the currently planned schedule. They are done in half year apart.

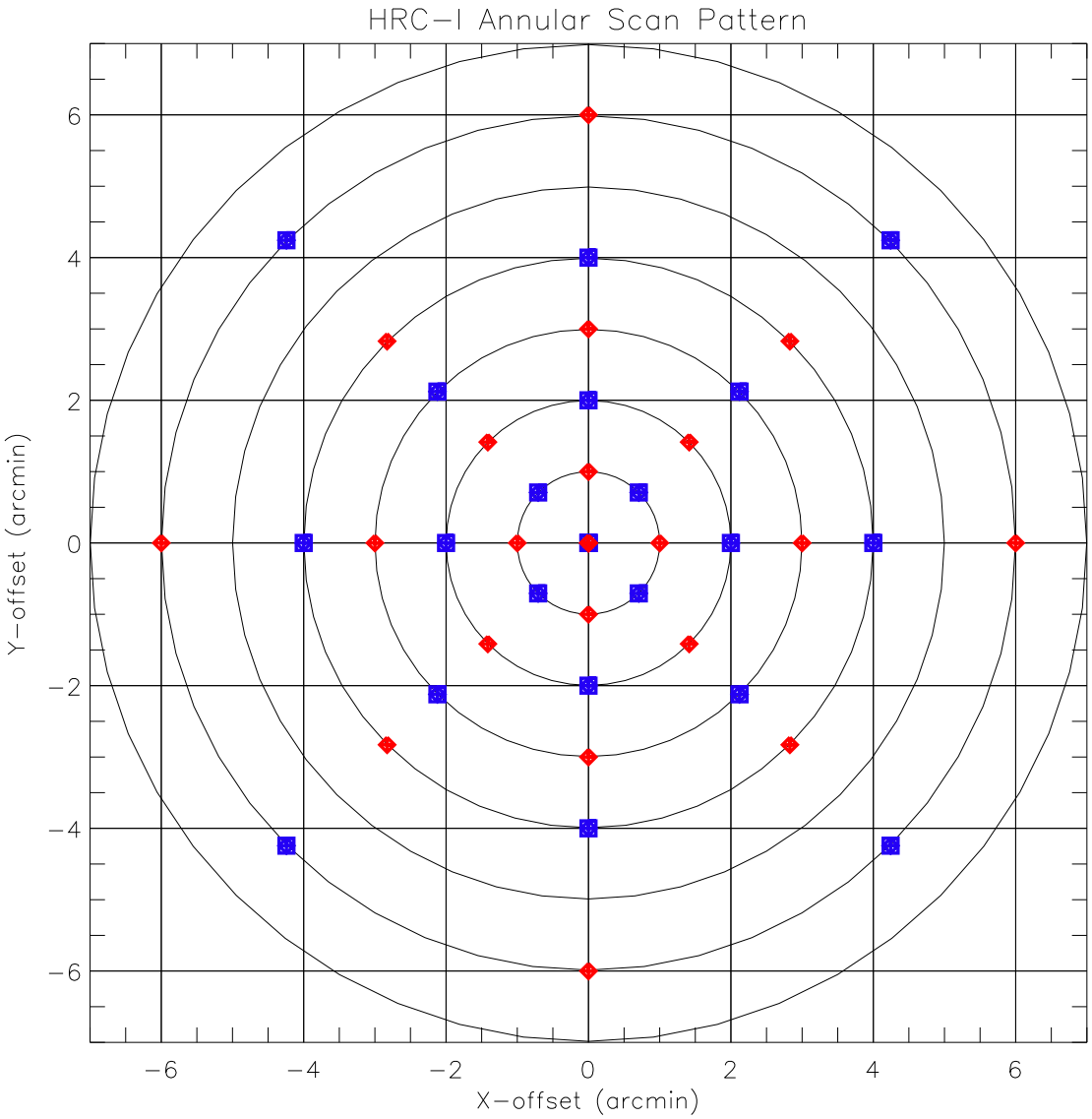

Figure 31: New annular scan pattern of HRC-I measurements of ArLac. The scan is divided into two groups of 21 observations each. The red diamonds indicate the first group; the blue squares indicate the second group.

References

[Zhao (2004)] Zhao, Ping "Chandra Telescope Optical Axis", Chandra Calibration Workshop, 2004, Cambridge, MA
http://cxc.cfa.harvard.edu/ccw/proceedings/04_proc/presentations/zhao

[Zhao (2005)] Zhao, Ping "Chandra Telescope Optical Axis and Aimpoint", Chandra Calibration Workshop, 2005, Cambridge, MA
http://cxc.cfa.harvard.edu/ccw/proceedings/05_proc/presentations/zhao

[Zhao (2006)] Zhao, Ping "Chandra Telescope Optical Axis and Aimpoint", Chandra X-ray Center Memorandum, 2006
http://cxc.harvard.edu/cal/Hrma/rsrc/Publish/Optics/OpticalAxisAndAimpoint/opt_axis_memo.pdf

[Zhao (2007)] Zhao, Ping "Chandra Telescope Optical Axis and Aimpoint", Chandra Calibration Workshop, 2007, Huntsville AL
http://cxc.cfa.harvard.edu/ccr/proceedings/07_proc/presentations/zhao

[Zhao (2009)] Zhao, Ping "The Quality and Stability of Chandra Telescope Pointing and Spatial Resolution", Chandra Calibration Review, 2009 Boston, MA
http://cxc.harvard.edu/ccr/proceedings/2009/presentations/zhao

[Zhao (2011)] Zhao, Ping "Chandra Aimpoint Drift and Default Offsets", Chandra X-ray Center Memorandum, 2011
http://cxc.harvard.edu/cal/Hrma/rsrc/Publish/Optics/OpticalAxisAndAimpoint/aimpoint_memo_2011

[Zhao (2012a)] Zhao, Ping "Chandra X-ray Observatory Aimpoint and Optical Axis", AAS 219th meeting, 2012, Bull.Am.Astro.Soc. 219, 446.01

[Zhao (2012b)] Zhao, Ping "The Quality and Stability of Chandra Telescope Pointing and Spacial Resolution", AAS 220th meeting, 2012, Bull.Am.Astro.Soc. 220, 122.05

[Zhao (2012c)] Zhao, Ping "Chandra Optical Axis, Aimpoint and Their Drifts", Chandra X-ray Center Memorandum, 2012
http://cxc.harvard.edu/cal/Hrma/rsrc/Publish/Optics/OpticalAxisAndAimpoint/oxap_memo_2012.pdf

[Zhao (2013)] Zhao, Ping "Chandra Optical Axis, Aimpoint and Their Drifts", Chandra X-ray Center Memorandum, 2013
http://cxc.harvard.edu/cal/Hrma/rsrc/Publish/Optics/OpticalAxisAndAimpoint/oxap_memo_2013.pdf

[Zhao (2014a)] Zhao, Ping "Chandra X-ray Observatory Pointing and its Stability", AAS 223th meeting, 2014, Bull.Am.Astro.Soc. 223, 109.06

[Zhao (2014b)] Zhao, Ping "Chandra Optical Axis, Aimpoint and Their Drifts", HEAD 14th meeting, 2014, 116.09

[Zhao (2014c)] Zhao, Ping "Chandra Optical Axis, Aimpoint and Their Drifts", Chandra X-ray Center Memorandum, 2014
http://cxc.harvard.edu/cal/Hrma/rsrc/Publish/Optics/OpticalAxisAndAimpoint/oxap_memo_2014.pdf

[Zhao (2015a)] Zhao, Ping "Chandra X-ray Observatory Pointing Stability", 10th IACHEC meeting, Beijing, China, 2015

[Zhao (2015c)] Zhao, Ping "Chandra Optical Axis and Aimpoint", Chandra X-ray Center Memorandum, 2015
http://cxc.harvard.edu/cal/Hrma/rsrc/Publish/Optics/OpticalAxisAndAimpoint/oxap_memo_2015.pdf

[Zhao (2016a)] Zhao, Ping "Chandra X-ray Observatory Optical Axis and Aimpoint", AAS 227th meeting, 2016, Bull.Am.Astro.Soc. 227, 445.08

[Zhao (2016c)] Zhao, Ping "Chandra Optical Axis and Aimpoint", Chandra X-ray Center Memorandum, 2016
http://cxc.harvard.edu/cal/Hrma/rsrc/Publish/Optics/OpticalAxisAndAimpoint/oxap_memo_2016.pdf

[Zhao (2017a)] Zhao, Ping "The Quality and Stability of Chandra Telescope Spacial Resolution", HEAD 16th meeting, 2017, 103.06

[Zhao (2017b)] Zhao, Ping "Chandra Optical Axis and Aimpoint", Chandra X-ray Center Memorandum, 2017
http://cxc.harvard.edu/cal/Hrma/rsrc/Publish/Optics/OpticalAxisAndAimpoint/oxap_memo_2017.pdf

[Zhao (2018a)] Zhao, Ping "The Stability of Chandra Telescope Pointing and Spacial Resolution", AAS 231th meeting, 2018, Bull.Am.Astro.Soc. 231, 447.09

[Zhao (2018b)] Zhao, Ping "Chandra Optical Axis and Aimpoint", Chandra X-ray Center Memorandum, 2018
http://cxc.harvard.edu/cal/Hrma/rsrc/Publish/Optics/OpticalAxisAndAimpoint/oxap_memo_2018.pdf

[Zhao (2019a)] Zhao, Ping "Chandra X-ray Observatory Optical Axis and Aimpoint", HEAD 17th meeting, 2019, 109.30

[Zhao (2019b)] Zhao, Ping. "Chandra X-ray Observatory Optical Axis, Aimpoint and Pointing Stability", 2019, 14th IACHEC meeting, Shonan Village Center, Japan
http://iachec.scripts.mit.edu/meetings/2019/presentations/sessionV_Zhao.pdf